F.W.O.-onderzoeksproject G.0200.01

Hydrodynamica en sedimenttransport.

Fundamentele aspecten bij een duurzaam beheer van zandige kusten

HYDRODYNAMICS AND SEDIMENT TRANSPORT

FUNDAMENTAL ASPECTS RELATED TO SUSTAINABLE MANAGEMENT OF SANDY COASTS

Technical Report no. 2

NUMERICAL SIMULATION OF TURBULENT BOUNDARY LAYERS IN OSCILLATORY FLOWS OVER PLANE BEDS

Author : T. De Mulder

Date : 19 September 2001

LABORATORIUM voor HYDRAULICA

K.U.LEUVEN

LABORATORIUM voor HYDRAULICA

UNIVERSITEIT GENT

WATERBOUWKUNDIG LABORATORIUM

BORGERHOUT

ABSTRACT

In this report, a one dimensional, vertical (1DV) hydrodynamic model is presented which describes the turbulent boundary layer flow over plane and hydraulically rough beds under the influence of combined (colinear) oscillatory and current flows in the freestream above the boundary layer.

The numerical approach to solve the governing equations and boundary conditions is carefully described, including some turbulence modelling aspects related to the mixing-length model and the $k-\varepsilon$ model.

Based on the described hydrodynamic model and numerical approach, a computer code is developed, which allows to study several aspects of (interacting) wave and current boundary layers without excessive computational costs.

Some testcases are presented, in order to provide a first testing of the code through comparison of the numerical predictions with published experimental and/or numerical data. The agreement between the results and the published data is satisfactory. Other testcases are merely presented to give an overview of the capabilities of the code.

Prospects for future research with the developed 1DV model and computer code are indicated.

1 INTRODUCTION

In the present report, an overview will be given of some work carried out in the frame of the FWO-Research Project G.0200.01, which focuses on hydrodynamics and sand transport in coastal environments.

The present work deals with numerical simulation of the hydrodynamics in turbulent oscillating flows over plane beds:

- Numerical simulation implies that the equations and boundary conditions which govern the flow will be discretized in space and time and will be solved by means of a computer programme which has been developed in the present work.
- Only hydrodynamics is considered, i.e. the first and necessary step for (future extension to) modelling of sand transport under influence of the considered flows. Consequently, no effects of large sediment concentrations on the fluid density or on the turbulence parameters are taken into account.
- Turbulent flows are considered, hence an important part of the work deals with turbulence modelling.
- Oscillatory flows are considered. These are typically studied in oscillating wave tunnels, in which the flow is uniform in the flow direction without any vertical orbital velocities. The latter characteristics will allow the use of a one-dimensional, vertical (1DV) model to describe the hydrodynamics. Obviously, the aforementioned flow characteristics of oscillatory flows are in contrast to the situation under progressive surface waves (which are common in coastal environments and which are typically studied in laboratory wave flumes). Nevertheless, the oscillating motion in oscillatory flows (and the associated 1DV-model) can be considered to be a good approximation for the near-bed flow under surface waves if (a) the horizontal flow velocity is small compared to the wave celerity and (b) the water depth is small compared to the wave length (Dohmen-Janssen, 1999). Notice that boundary layer streaming (i.e. the production of a net flow in a thin near-wall layer under progressive surface waves) is absent in oscillatory flows.
- Different types of flows are considered: pure oscillatory flows (like e.g. symmetric waves, asymmetric waves, wave groups), steady currents, combined (colinear) oscillatory flows and currents. Hence, wave boundary layers and/or current boundary layers will be studied.
- Plane beds are considered, hence the effects of large ripples (i.e. ripples which are large in comparison to the dimensions of the bed grains, and over which the flow separates) are not accounted for. The bed roughness is assumed to depend on the median grain size of the bed material.

Similar work has been undertaken before by several researchers. The reader is referred to e.g. (Justesen, 1988), (Justesen, 1991), (Savioli and Justesen, 1997) and earlier references therein. Consequently, the objective of the present work is not to present a completely new approach to the study of wave and current boundary layers, although some detailed aspects might differ from the aforementioned references.

The present work rather aims at the development of a computer code which can be used afterwards to study several aspects of (interacting) wave and current boundary layers, without excessive computational costs. As such it will be beneficial in the on-going FWO-research project which aims at a combined numerical and experimental study of the hydrodynamics (and sand transport) in coastal areas. On the other hand, it should be useful as a didactical tool to familiarize students with (oscillatory) boundary layer flows.

Additionally, the present work wants to provide a comprehensive description of popular turbulence models and their numerical discretization, which might be of use for people who are less familiar with these topics.

In chapter 2 of the present report, the underlying hydrodynamic model will be presented. The numerical approach to solve the governing equations and boundary conditions is presented in chapter 3. Based on the description of the hydrodynamic model and the numerical approach, a computer code has been developed. In order to provide a first testing of the code some testcases are simulated in chapter 4 and the present results will be compared to published experimental and/or numerical results. Other testcases will be simply dealt with in order to give an overview of the capabilities of the present code. Finally, a summary and ideas for future research are presented in chapter 5.

2 HYDRODYNAMIC MODEL

The oscillatory boundary layer flow is described as a uniform unsteady turbulent boundary layer using a one-dimensional vertical (1DV) schematization, with no vertical components of the turbulent mean velocity (i.e. contrary to progressive surface waves where water particles make orbital movements and consequently have vertical velocity components).

2.1 Domain

Consider a vertical, upward pointing z-axis. The domain then extends from $z=z_o$ (i.e. a near-bed reference level which depends on the roughness of the bed, see 2.3.1.1) up to $z=z_\infty$ (i.e. the height of the domain where boundary layer effects are assumed to have vanished and freestream conditions apply). The domain has no extension along the horizontal x-axis, since the flow is assumed to be uniform.

2.2 Equations

2.2.1 Momentum equation

From the Reynolds-averaged Navier-Stokes equations, one can derive the following momentum equation in case of a uniform, 1DV flow:

$$\frac{\partial U}{\partial t} = -\frac{1}{\rho}\frac{\partial p}{\partial x} + \frac{\partial}{\partial z}\left[\nu \frac{\partial U}{\partial z} - \overline{u'w'}\right]$$

in which t represents time, x and z are the horizontal and vertical coordinate axes respectively, U is the horizontal component of the turbulent mean velocity, u' and w' are the horizontal and vertical velocity fluctuations respectively, ρ is the fluid density, p is the pressure and ν is the kinematic viscosity.

Application of the Boussinesq hypothesis (or eddy viscosity hypothesis) for the Reynolds stress, allows to rewrite the momentum equation within the boundary layer as follows:

$$\frac{\partial U}{\partial t} = -\frac{1}{\rho}\frac{\partial p}{\partial x} + \frac{\partial}{\partial z}\left[(\nu + \nu_t)\frac{\partial U}{\partial z}\right]$$

in which ν_t is the eddy viscosity.

Considering the molecular viscosity effects to be negligible in comparison to the turbulence effects (see APPENDIX A), the momentum equation finally becomes

$$\frac{\partial U}{\partial t} = -\frac{1}{\rho}\frac{\partial p}{\partial x} + \frac{\partial}{\partial z}\left(\nu_t \frac{\partial U}{\partial z}\right).$$

2.2.1.1 Pressure gradient

In thin boundary layer theory, it is assumed that the ambient pressure (i.e. the pressure in the freestream above the boundary layer) penetrates the entire boundary layer undisturbedly. Therefore, the horizontal pressure gradient term in the abovementioned boundary layer momentum equation equals the horizontal gradient of the ambient pressure. In the subsequent paragraphs will be explained which form the latter pressure gradient term takes for different types of flow.

2.2.1.1.1 Pure oscillatory flow

In case of a pure oscillatory flow, the horizontal pressure gradient term can be found by applying the momentum equation to the freestream flow above the boundary layer. In the freestream, the shear stresses are assumed to vanish and the velocity approaches the freestream velocity U_∞. Consequently, the momentum equation above the boundary layer can be written as

$$\frac{\partial U_\infty}{\partial t} = -\frac{1}{\rho}\frac{\partial p}{\partial x},$$

which allows to calculate the horizontal pressure gradient term, if the freestream acceleration is known. The latter condition is fulfilled when simulating a particular oscillatory flow characterized by a prescribed timeseries of the freestream velocity, like e.g. a sinusoidal wave with $U_\infty(t) = U_o \sin(\omega t)$.

2.2.1.1.2 Steady current

In case of a steady uniform current, the pressure gradient term is related to the slope S of the energy line:

$$-\frac{1}{\rho}\frac{\partial p}{\partial x} = gS$$

in which g is the gravitational acceleration. See also APPENDIX B.

2.2.1.1.3 Combined current and oscillatory flow

In case of a combined (colinear) current and oscillatory flow, the horizontal pressure gradient is expressed as:

$$-\frac{1}{\rho}\frac{\partial p}{\partial x} = \frac{\partial U_\infty}{\partial t} + gS\,.$$

2.2.2 Turbulence model

To close the momentum equation, a turbulence model is required. The eddy viscosity ν_t is usually supposed to be proportional to the product of a turbulent velocity scale $\tilde{u}$ and a turbulent length scale ℓ:

$$\nu_t \propto \tilde{u}\,\ell\,.$$

Turbulence models differ in the way $\tilde{u}$ and ℓ are defined and in the number (e.g. 0, 1, 2,…) of partial differential equations (PDE) which are required to calculate those turbulent scales.

In the following sections, two turbulence models which are considered in the present work will be introduced.

2.2.2.1 Mixing-length model

Based on Prandtl's mixing-length theory, the turbulent length scale is defined by means of the mixing-length:

$$\ell = \kappa z$$

in which z is the distance to the wall and κ is von Karman's constant which is usually taken as equal to 0.4.

The turbulent velocity scale is then defined in terms of the mixing-length and the mean velocity gradient as follows

$$\tilde{u} = \ell \left| \frac{\partial U}{\partial z} \right|$$

so that

$$\nu_t = (\kappa z)^2 \left| \frac{\partial U}{\partial z} \right| .$$

Notice that the mixing-length model is a zero-equation model since no extra PDE has to be solved in order to express the eddy viscosity in terms of known, grid-resolved quantities (c.q. the gradient of the turbulent mean velocity).

Notice also that the eddy viscosity is only a function of the local flow conditions, i.e. turbulence is assumed to be at a local equilibrium (and consequently is not influenced by the surrounding flow), i.e. the rates of production and dissipation of turbulence are in near-balance.

2.2.2.2 Two-equation k-ε model

Be k the turbulent kinetic energy per unit mass (units: $\mathrm{m}^2/\mathrm{s}^2$),

$$k = \frac{1}{2}\left(\overline{u'^2} + \overline{v'^2} + \overline{w'^2} \right),$$

and ε the rate of dissipation of turbulent kinetic energy (units: $\mathrm{m}^2/\mathrm{s}^3$).

The turbulent velocity scale can then be defined as follows

$$\tilde{u} \propto k^{1/2},$$

whereas the turbulent length scale is usually expressed (based on dimensional analysis and considerations for equilibrium turbulent flows, see e.g. (Ferziger and Peric, 1996)) as

$$\ell \propto \frac{k^{3/2}}{\varepsilon}$$

so that

$$\nu_t = c_\mu \frac{k^2}{\varepsilon},$$

in which c_μ is a constant.

Contrary to the mixing-length model, the assumption of turbulence being in a local equilibrium is not made in case of the k-ε model. The local turbulent scales can be influenced by the surrounding flow, since a transport equation (PDE) for both k and ε is provided for:

$$\frac{\partial k}{\partial t} = \frac{\partial}{\partial z}\left[\left(\frac{\nu_t}{\sigma_k}\right)\frac{\partial k}{\partial z}\right] + P - \varepsilon$$

$$\frac{\partial \varepsilon}{\partial t} = \frac{\partial}{\partial z}\left[\left(\frac{\nu_t}{\sigma_\varepsilon}\right)\frac{\partial \varepsilon}{\partial z}\right] + c_{\varepsilon 1}\frac{\varepsilon}{k}P - c_{\varepsilon 2}\frac{\varepsilon^2}{k}$$

in which $c_{\varepsilon 1}$, $c_{\varepsilon 2}$, σ_k and σ_ε are constants.

One should be aware that these transport equations constitute a model which has been derived from the exact transport equations for k and ε through various (often very crude) assumptions. Those approximations are necessary to eliminate unknown higher-order correlations between turbulent velocity and pressure fluctuations which are present in the exact transport equations (i.e. a fact which illustrates the so-called turbulence closure problem). See e.g. (Ferziger and Peric, 1996).

In the above equations, P denotes the production rate of turbulent kinetic energy. P represents the work performed by the shear stress ($\tau_t/\rho = -\overline{u'w'}$) against the mean flow strain rate ($= \partial U/\partial z$), see e.g. (Abbott and Basco, 1989):

$$P = -\overline{u'w'}\frac{\partial U}{\partial z}.$$

Introducing the eddy viscosity formulation for the Reynolds stress, it becomes

$$P = \nu_t\left(\frac{\partial U}{\partial z}\right)^2.$$

The standard set of constants for the k-ε model are given in Table 2-1. One should be aware that these constants have been derived by tuning the model to obtain the values of measured data in case of simple experimental (laboratory) flow conditions (Abbott and Basco, 1989).

c_μ	$c_{\varepsilon 1}$	$c_{\varepsilon 2}$	σ_k	σ_ε
0.09	1.44	1.92	1.00	1.30

Table 2-1 : Standard set of constants for the k-ε model

2.3 Boundary conditions

2.3.1 Velocity

Velocity boundary conditions at the bed and at the top of the domain are required in order to solve the momentum equation.

2.3.1.1 At the bed

The bed is treated as a hydraulically rough wall with an equivalent Nikuradse roughness height k_n. (see APPENDIX C). Usually, k_n is related to the median sediment grain size:

$$k_n = 2.5 d_{50}\,.$$

Following Nikuradse, a no-slip velocity boundary condition is then applied at the zero-velocity reference level $z=z_o$ where $z_o=k_n/30$ (see also APPENDIX E):

$$U(z_o,t)=0.$$

Notice that this boundary condition is of the so-called homogenous Dirichlet type (see APPENDIX D).

2.3.1.2 At the top of the domain

At the top of the flow domain, the (time-dependent) freestream velocity is usually imposed:

$$U(z_\infty,t)=U_\infty(t),$$

i.e. a Dirichlet type condition (see APPENDIX D).

Alternatively, one could impose a zero normal velocity gradient (i.e. a so-called homogeneous Neumann type condition, see APPENDIX D):

$$\left(\frac{\partial U}{\partial z}\right)_{z=z_\infty} = 0\,.$$

The physical meaning of the latter boundary condition is imposing a zero shear stress,

$$-\overline{u'w'} = \left[\nu_t\left(\frac{\partial U}{\partial z}\right)\right]_{z=z_\infty} = 0,$$

corresponding to a shearless freestream above the boundary layer.

2.3.2 Turbulent variables

In case of the k-ε model, boundary conditions at the bed and at the top of the domain are required in order to solve the transport equations for k and ε.

2.3.2.1 At the bed

Under some assumptions, and making use of the definition of the wall friction velocity

$$u_* = \sqrt{\tau_w / \rho}\ ,$$

in which τ_w denotes the wall shear stress, one can derive (see APPENDIX F) the following boundary conditions for k and ε:

$$k(z_o, t) = \frac{{u_*}^2}{\sqrt{c_\mu}}$$

$$\varepsilon(z_o, t) = \frac{{u_*}^3}{\kappa z_o}\ .$$

Notice that these boundary conditions are of the Dirichlet type (see APPENDIX D).

In order to apply these boundary conditions, one should be able to calculate the friction velocity. In literature, the following relation is often adopted:

$$u_* = \sqrt{\left(\nu_t \left| \frac{\partial U}{\partial z} \right| \right)_{z=z_o}}\ .$$

An alternative way to determine the friction velocity, is based on the assumption of a logarithmic velocity profile,

$$\frac{U(z)}{u_*} = \frac{1}{\kappa} \ln\left(\frac{z}{z_o} \right),$$

from which one can retrieve the friction velocity if the velocity U_1 at the first grid point (at $z=z_1$) away from the wall (at $z=z_o$) is known:

$$u_* = \frac{\kappa U_1}{\ln(z_1 / z_o)}\ .$$

2.3.2.2 At the top of the domain

At the top of the domain, so-called symmetry conditions are usually applied:

$$\frac{\partial k}{\partial z} = \frac{\partial \varepsilon}{\partial z} = 0 \ \text{ at } z=z_{\infty}.$$

Notice that these boundary conditions are of the homogeneous Neumann type (see APPENDIX D).

2.4 Summary

In Table 2-2, an overview is given of the alternative models which are considered in the present work to describe turbulent flow over a plane and hydraulically rough bed with a zero-velocity reference level z_o.

Model	Eddy-viscosity	Equations	BC at bed	BC at top of domain
Mixing-length	$\nu_t = (\kappa z)^2 \left\lvert \frac{\partial U}{\partial z} \right\rvert$	$\frac{\partial U}{\partial t} = -\frac{1}{\rho}\frac{\partial p}{\partial x} + \frac{\partial}{\partial z}\left(\nu_t \frac{\partial U}{\partial z}\right)$	$U(z_o,t) = 0$	$U(z_\infty,t) = U_\infty(t)$ or $\left(\frac{\partial U}{\partial z}\right)_{z=z_\infty} = 0$
$k-\varepsilon$	$\nu_t = c_\mu \frac{k^2}{\varepsilon}$	$\frac{\partial U}{\partial t} = -\frac{1}{\rho}\frac{\partial p}{\partial x} + \frac{\partial}{\partial z}\left(\nu_t \frac{\partial U}{\partial z}\right)$ $\frac{\partial k}{\partial t} = \frac{\partial}{\partial z}\left[\left(\frac{\nu_t}{\sigma_k}\right)\frac{\partial k}{\partial z}\right] + P - \varepsilon$ $\frac{\partial \varepsilon}{\partial t} = \frac{\partial}{\partial z}\left[\left(\frac{\nu_t}{\sigma_\varepsilon}\right)\frac{\partial \varepsilon}{\partial z}\right] + c_{\varepsilon 1}\frac{\varepsilon}{k}P - c_{\varepsilon 2}\frac{\varepsilon^2}{k}$	$U(z_o,t) = 0$ $k(z_o,t) = \frac{{u_*}^2}{\sqrt{c_\mu}}$ $\varepsilon(z_o,t) = \frac{{u_*}^3}{\kappa z_o}$ with $u_* = \sqrt{\left(\nu_t \left\lvert \frac{\partial U}{\partial z} \right\rvert\right)_{z=z_o}}$ or $u_* = \frac{\kappa U_1}{\ln(z_1/z_o)}$	$U(z_\infty,t) = U_\infty(t)$ or $\left(\frac{\partial U}{\partial z}\right)_{z=z_\infty} = 0$ $\left(\frac{\partial k}{\partial z}\right)_{z=z_\infty} = 0$ $\left(\frac{\partial \varepsilon}{\partial z}\right)_{z=z_\infty} = 0$

Table 2-2 : Overview of alternative models considered in the present work for turbulent flow over a plane and hydraulically rough bed

3 NUMERICAL APPROACH

3.1 Unsteady diffusion equation

The momentum equation, as well as the k- and ε-transport equations can be written in the following, general form:

$$\frac{\partial \varphi}{\partial t} = \frac{\partial}{\partial z}\left(K \frac{\partial \varphi}{\partial z} \right) + Q \,,$$

i.e. an unsteady diffusion equation with variable φ, diffusivity K and source/sink-term Q, as shown in Table 3-1.

	variable φ	diffusivity K	source/sink term Q
momentum equation	U	ν_t	$-\frac{1}{\rho}\frac{\partial p}{\partial x} = gS + \frac{\partial U_\infty}{\partial t}$
k-equation	k	$\frac{\nu_t}{\sigma_k}$	$P - \varepsilon$ where $P = \nu_t \left(\frac{\partial U}{\partial z} \right)^2$
ε-equation	ε	$\frac{\nu_t}{\sigma_\varepsilon}$	$c_{\varepsilon 1} \frac{\varepsilon}{k} P - c_{\varepsilon 2} \frac{\varepsilon^2}{k}$

Table 3-1 : Translation of equations into framework of an unsteady diffusion equation with source/sink-term

Notice that in case of the k- and ε-equations, Q is a nonlinear function of φ since $P = \nu_t \left(\frac{\partial U}{\partial z} \right)^2 = c_\mu \frac{k^2}{\varepsilon} \left(\frac{\partial U}{\partial z} \right)^2$.

The aforementioned unsteady diffusion equation will be solved numerically based upon a finite difference discretization in space and in time.

3.2 Grid

The interval (z_o, z_∞) along the z-axis will be divided into a set of N segments defined by the grid points $\{z_i\}_{i=0,N}$, where $z_0 = z_o$ (=zero-velocity level at bed) and $z_N = z_\infty$ (=top of domain). See Figure 3-1.

In order to accurately resolve the boundary layer effects close to the 'wall', it is preferable to have small grid segments in that area, whereas larger grid segments are acceptable close to the top of the domain where boundary layer effects are vanishing.

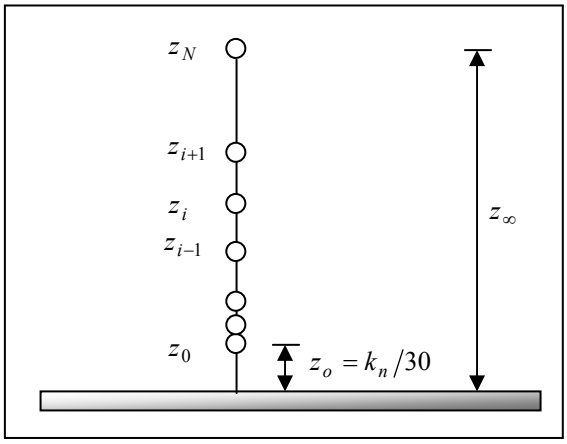

Figure 3-1 : Definition of vertical grid

Therefore, grid stretching will be allowed for, i.e. the length of consecutive grid segments will be allowed to grow with a (constant, user specified) stretching factor R :

$$(z_{i+1} - z_i)/(z_i - z_{i-1}) = R\,.$$

Some further details of the grid generation are given in APPENDIX G.

For accuracy reasons (see section 3.4.1), the abovementioned stretching factor should not deviate too much from unity (e.g. 1.05 seems appropriate).

Notice that for each segment *i*, which is delimited by grid points z_{i-1} and z_i, the center of the segment will be denoted as $z_{i-1/2}$.

The variables φ_i (like e.g. U_i, k_i, ε_i) and related quantities (like e.g. the eddy-viscosity ν_{ti}) will be stored at the grid points z_i.

3.3 Discretization in time

3.3.1 Implicit formulation

In the present work, the unsteady diffusion equation will be discretized in time based upon an implicit formulation:

$$\frac{\varphi^{n+1} - \varphi^n}{\Delta t} = \theta\left[\frac{\partial}{\partial z}\left(K\frac{\partial \varphi}{\partial z}\right) + Q\right]^{n+1} + (1-\theta)\left[\frac{\partial}{\partial z}\left(K\frac{\partial \varphi}{\partial z}\right) + Q\right]^{n},$$

or:

$$\frac{\varphi^{n+1} - \varphi^n}{\Delta t} = \left(\theta\left[\frac{\partial}{\partial z}\left(K\frac{\partial \varphi}{\partial z}\right)\right]^{n+1} + (1-\theta)\left[\frac{\partial}{\partial z}\left(K\frac{\partial \varphi}{\partial z}\right)\right]^{n}\right) + \left(\theta Q^{n+1} + (1-\theta)Q^n\right)$$

in which :

- the first and second term in the right-hand-side represent the diffusion term and the source/sink-term respectively,
- Δt is the timestep,

- n indicates the previous time level, $t = n\Delta t$, at which φ^n is known,
- $n+1$ is the new time level, $t = (n+1)\Delta t$, at which φ^{n+1} is unknown (and is to be calculated),
- θ is a weighting coefficient, such that a fully explicit formulation is retrieved if $\theta = 0$, whereas a fully implicit formulation corresponds to $\theta = 1$.

Notice that the choice of the timestep requires special attention. For reasons of accuracy, the timestep should not exceed a tenth (or so) of the wave period which corresponds to the oscillating flow one wants to simulate.

Depending on the choice of the weighting coefficient θ, however, one can be obliged to adopt much smaller timesteps than the one derived based upon accuracy reasons. Indeed, explicit formulations lead to problems of numerical stability unless a (prohibitively) small timestep is applied. The more implicit a formulation, the longer timestep that can be chosen while still obtaining stable numerical solutions.

Therefore, fully-implicit ($\theta = 1$) or semi-implicit ($\theta = 0.5$) formulations are advocated in the present work. In principle, the fully-implicit scheme is first order accurate in time, whereas the semi-implicit formulation would be second order accurate in time (Cranck-Nicholson scheme), at least in case of a pure diffusion equation with constant coefficients. In practice, the fully-implicit formulation is often adopted since it allows a larger timestep than the semi-implicit formulation.

3.3.2 Source/sink term

Some comments should be added concerning the discretization in time of the (nonlinear) source/sink-term Q.

For the momentum equation, a straightforward discretization of the linear Q-term gives:

$$Q^{n+1} = Q^n = gS + \frac{U_\infty^{n+1} - U_\infty^n}{\Delta t}.$$

For the k- and ε-equations, however, the nonlinear Q-terms require special care.

Thus, for the k-equation one has:

$$Q^n = P^n - \varepsilon^n,$$

$$Q^{n+1} = P^{n+1} - \varepsilon^{n+1} \approx P^n - \left(\frac{c_\mu k^2}{\nu_t}\right)^{n+1} \approx P^n - \left(\frac{c_\mu k}{\nu_t}\right)^n k^{n+1}.$$

This particular linearization - which ensures the coefficient in front of k^{n+1} is always negative - is chosen in order to increase the diagonal dominance of the resulting system, as will become clear in sections 3.4.2 and 3.5.

In a similar way, one has for the ε-equation:

$$Q^n = \left(c_{\varepsilon 1}\frac{\varepsilon}{k}P\right)^n - \left(c_{\varepsilon 2}\frac{\varepsilon^2}{k}\right)^n$$

$$Q^{n+1} = \left(c_{\varepsilon 1} \frac{\varepsilon}{k} P \right)^{n+1} - \left(c_{\varepsilon 2} \frac{\varepsilon^2}{k} \right)^{n+1} \approx \left(c_{\varepsilon 1} \frac{\varepsilon}{k} P \right)^{n} - \left(c_{\varepsilon 2} \frac{\varepsilon}{k} \right)^{n} \varepsilon^{n+1} .$$

Again, the particular linearization - which ensures the coefficient in front of ε^{n+1} is always negative - is chosen in order to increase the diagonal dominance of the resulting system.

3.4 Discretization in space

3.4.1 Diffusion term

The diffusion term will be discretized as follows:

$$\left[\frac{\partial}{\partial z} \left(K \frac{\partial \varphi}{\partial z} \right) \right]^{n+1} = \frac{K^n_{i+1/2} \left(\frac{\varphi_{i+1} - \varphi_i}{z_{i+1} - z_i} \right)^{n+1} - K^n_{i-1/2} \left(\frac{\varphi_i - \varphi_{i-1}}{z_i - z_{i-1}} \right)^{n+1}}{z_{i+1/2} - z_{i-1/2}},$$

$$\left[\frac{\partial}{\partial z} \left(K \frac{\partial \varphi}{\partial z} \right) \right]^{n} = \frac{K^n_{i+1/2} \left(\frac{\varphi_{i+1} - \varphi_i}{z_{i+1} - z_i} \right)^{n} - K^n_{i-1/2} \left(\frac{\varphi_i - \varphi_{i-1}}{z_i - z_{i-1}} \right)^{n}}{z_{i+1/2} - z_{i-1/2}} .$$

Notice that the diffusivities are required at the segment center points $z_{i-1/2}$, whereas the information is stored at the grid points z_i. Therefore, simple arithmetic averaging will be applied:

$$K^n_{i-1/2} = \left(K^n_{i-1} + K^n_i \right) / 2 ,$$

$$K^n_{i+1/2} = \left(K^n_i + K^n_{i+1} \right) / 2 .$$

For a uniform grid, the aforementioned discretization is second order accurate in space. In case of a stretched grid, however, one can preserve the accuracy only if the stretching factor R deviates not too much from unity (e.g. 1.05).

If the abovementioned discretization of the diffusion term is inserted into the time-discretized unsteady diffusion equation, one can obtain (after rearrangement) the following relation between the 3 neighbouring unknowns $\varphi^{n+1}_{i-1}, \varphi^{n+1}_i, \varphi^{n+1}_{i+1}$ at the new time level *n+1:*

$$A_i \varphi^{n+1}_{i-1} + B_i \varphi^{n+1}_i + C_i \varphi^{n+1}_{i+1} = F_i ,$$

in which:

$$A_i = - \frac{\theta \Delta t}{\left(z_{i+1/2} - z_{i-1/2} \right)} \left(\frac{K^n_{i-1/2}}{z_i - z_{i-1}} \right)$$

$$B_i = 1 + \frac{\theta \Delta t}{\left(z_{i+1/2} - z_{i-1/2} \right)} \left(\frac{K^n_{i+1/2}}{z_{i+1} - z_i} + \frac{K^n_{i-1/2}}{z_i - z_{i-1}} \right)$$

$$C_i = -\frac{\theta\Delta t}{\left(z_{i+1/2} - z_{i-1/2}\right)}\left(\frac{K^n_{i+1/2}}{z_{i+1} - z_i}\right)$$

$$F_i = \varphi^n_i + \frac{\left(1-\theta\right)\Delta t}{\left(z_{i+1/2} - z_{i-1/2}\right)}\left(K^n_{i+1/2}\frac{\varphi^n_{i+1} - \varphi^n_i}{z_{i+1} - z_i} - K^n_{i-1/2}\frac{\varphi^n_i - \varphi^n_{i-1}}{z_i - z_{i-1}}\right).$$

For each of the unknowns φ^{n+1}_i one can derive a similar algebraic relation. This set of relations leads to a system which is characterized by a tridiagonal matrix:

$$\begin{pmatrix} \ddots & \ddots & \ddots & & & & \\ & A_{i-1} & B_{i-1} & C_{i-1} & & & \\ & & A_i & B_i & C_i & & \\ & & & A_{i+1} & B_{i+1} & C_{i+1} & \\ & & & & \ddots & \ddots & \ddots \end{pmatrix}\begin{pmatrix} \vdots \\ \varphi^{n+1}_{i-1} \\ \varphi^{n+1}_i \\ \varphi^{n+1}_{i+1} \\ \vdots \end{pmatrix} = \begin{pmatrix} \vdots \\ F_{i-1} \\ F_i \\ F_{i+1} \\ \vdots \end{pmatrix}.$$

3.4.2 Source/sink term

The aforementioned coefficients A_i, B_i, C_i and F_i only account for the diffusion term. To account for the source/sink term, the following modifications should be made.

For the momentum equation one has:

$$F_i = \varphi^n_i + \frac{\left(1-\theta\right)\Delta t}{\left(z_{i+1/2} - z_{i-1/2}\right)}\left(K^n_{i+1/2}\frac{\varphi^n_{i+1} - \varphi^n_i}{z_{i+1} - z_i} - K^n_{i-1/2}\frac{\varphi^n_i - \varphi^n_{i-1}}{z_i - z_{i-1}}\right) + \Delta t\left(gS + \frac{U^{n+1}_\infty - U^n_\infty}{\Delta t}\right).$$

For the k-equation one has:

$$B_i = 1 + \frac{\theta\Delta t}{\left(z_{i+1/2} - z_{i-1/2}\right)}\left(\frac{K^n_{i+1/2}}{z_{i+1} - z_i} + \frac{K^n_{i-1/2}}{z_i - z_{i-1}}\right) + \theta\Delta t\left(\frac{c_\mu k}{\nu_t}\right)^n,$$

$$F_i = \varphi^n_i + \frac{\left(1-\theta\right)\Delta t}{\left(z_{i+1/2} - z_{i-1/2}\right)}\left(K^n_{i+1/2}\frac{\varphi^n_{i+1} - \varphi^n_i}{z_{i+1} - z_i} - K^n_{i-1/2}\frac{\varphi^n_i - \varphi^n_{i-1}}{z_i - z_{i-1}}\right) + \Delta t P^n - \left(1-\theta\right)\Delta t\varepsilon^n,$$

in which

$$P^n = \left[\nu_t\left(\frac{U_{i+1} - U_{i-1}}{z_{i+1} - z_{i-1}}\right)^2\right]^n.$$

Notice that the diagonal coefficient B_i indeed increases, i.e. the system becomes more diagonal dominant since $\left(c_\mu k/\nu_t\right)^n \geq 0$ due to the particular linearization (introduced in section 3.3.2) of the source/sink term.

In a similar way, one has for the ε-equation:

$$B_i = 1 + \frac{\theta\Delta t}{\left(z_{i+1/2} - z_{i-1/2}\right)}\left(\frac{K^n_{i+1/2}}{z_{i+1} - z_i} + \frac{K^n_{i-1/2}}{z_i - z_{i-1}}\right) + \theta\Delta t\left(\frac{c_{\varepsilon 2}\varepsilon}{k}\right)^n,$$

$$F_i = \varphi_i^n + \frac{(1-\theta)\Delta t}{(z_{i+1/2} - z_{i-1/2})}\left(K_{i+1/2}^n \frac{\varphi_{i+1}^n - \varphi_i^n}{z_{i+1} - z_i} - K_{i-1/2}^n \frac{\varphi_i^n - \varphi_{i-1}^n}{z_i - z_{i-1}} \right) + \Delta t\left(\frac{c_{\varepsilon 1}\varepsilon}{k} \right)^n P^n - (1-\theta)\Delta t\left(\frac{c_{\varepsilon 2}\varepsilon^2}{k} \right)^n .$$

Again the diagonal coefficient B_i indeed increases, i.e. the system becomes more diagonal dominant since $(c_{\varepsilon 2}\varepsilon/k)^n \geq 0$ due to the particular linearization (introduced in section 3.3.2) of the source/sink term.

3.4.3 Boundary conditions

Suppose that a Dirichlet type condition (see APPENDIX D) has to be applied in grid point z_0,

$$\varphi_0^{n+1} = \alpha_0 ,$$

in which α_0 is a prescribed value, then the corresponding row in the tridiagonal system becomes :

$$(A_0 \text{ not present}),\ B_0 = 1,\ C_0 = 0,\ F_0 = \alpha_0 .$$

If, on the contrary, a homogeneous Neumann type condition (see APPENDIX D) has to be imposed at grid point z_0,

$$\left(\frac{\partial \varphi}{\partial z} \right)_0^{n+1} = 0 ,$$

then the corresponding row in the tridiagonal system becomes :

$$(A_0 \text{ not present}),\ B_0 = 1,\ C_0 = -1,\ F_0 = 0 .$$

In a similar way, the boundary condition at grid point $z_N (= z_\infty)$ can be dealt with, and the corresponding row in the system can be determined: A_N, B_N, (C_N not present) and F_N.

Finally, the system to be solved becomes:

$$\begin{pmatrix} B_0 & C_0 & & & \\ \ddots & \ddots & \ddots & & \\ & A_i & B_i & C_i & \\ & & \ddots & \ddots & \ddots \\ & & & A_N & B_N \end{pmatrix} \cdot \begin{pmatrix} \varphi_0^{n+1} \\ \vdots \\ \varphi_i^{n+1} \\ \vdots \\ \varphi_N^{n+1} \end{pmatrix} = \begin{pmatrix} F_0 \\ \vdots \\ F_i \\ \vdots \\ F_N \end{pmatrix} .$$

3.5 Solution of tridiagonal systems

For every new time level $t = (n+1)\Delta t$, i.e. for every consecutive timestep, one should solve a similar tridiagonal system in order to obtain the unknown variables φ_i^{n+1}.

The well-known Thomas algorithm will be adopted. See e.g. pages 505-506 in (Hirsch, 1988). It can be shown that this algorithm will always converge if the tridiagonal system is diagonal dominant.

3.6 Initial conditions

In principle, the abovementioned timestepping procedure can start from any initial condition, while always leading to the same periodic solution when the transient part of the solution is damped out. Of course, the better the initial condition, the faster the transient part damps out.

In the present work, one can either start from an existing solution (i.e. the final solution to a previous boundary layer simulation) or one can adopt the relations given in APPENDIX H.

3.7 Convergence monitoring

In order to allow the transient part of the solution (which is due to the initial condition not being an exact solution to the posed problem) to damp out, the following approach is adopted.

Be T_{cycle} the timescale at which the (oscillating) freestream flow, $U_\infty(t)$, can be considered to be periodic. (In case of a non-oscillating, steady freestream current, an arbitrary T_{cycle} value can be specified.)

The numerical timestepping procedure will then be carried out during a timespan equal to a multiple N_{cycle} of T_{cycle}. If N_{cycle} is large enough, the numerical solution will eventually converge and the (requested) periodic solution is obtained.

In order to allow the user to monitor the convergence, some quantities will be calculated for each subsequent period T_{cycle}. Some further details of the present work are given in APPENDIX I.

If the numerical results do not seem to converge, then selection of a smaller timestep often cures the problem. If, on the other hand, no convergence problems are encountered, one might increase the timestep in order to speed-up the calculation procedure.

3.8 Selection of timestep and grid resolution

The reader should be aware that the present work is based upon numerical solution of discretized equations with a given, user-specified timestep and vertical grid resolution.

Even if a particular choice of timestep and grid resolution seems to give reasonable and converged results, it is good practice to verify whether the numerical results significantly change by adopting a smaller timestep and a finer grid.

4 TESTCASES

Based on the foregoing description of the hydrodynamic model and the numerical approach, a computer code has been developed. This chapter will present some results obtained with that code. The main objectives are:

- To have a first testing of the computer code, by running cases of which experimental data are available and/or of which numerical simulations by other researchers have been presented in literature.
- To give an overview of the capabilities of the computer code, by simply running testcases without thorough comparison to published experimental or numerical data.

4.1 Pure oscillatory flow

4.1.1 Sinusoidal wave

Jensen et al. (Jensen et al., 1989) investigated oscillatory boundary layers in sinusoidal waves through experiments in the water tunnel at the Technical University of Denmark.

In this section the sinusoidal wave experiment will be considered of which some characteristic parameters are listed below :

- velocity amplitude U_o=2 m/s, which corresponds to a root-mean-square velocity of $U_{rms} = U_o / \sqrt{2}$ =1.41 m/s,
- wave period T=9.72 s,
- equivalent Nikuradse roughness length k_n=0.84 mm.

This testcase will be simulated by imposing the following freestream velocity at $z=z_\infty=400k_n$=0.336m :

$$U_\infty(t) = U_o \sin(\omega t)$$

in which the angular frequency of oscillation is given by $\omega = 2\pi/T$. Be A the particle amplitude in the freestream oscillation, then the ratio of A to the roughness length k_n is given by:

$$\frac{A}{k_n} = \frac{U_o}{\omega k_n} \approx 3700.$$

In order to simulate the foregoing purely oscillating flow, the zero-velocity reference level is taken as $z_o = k_n / 30$. Between z_o and z_∞, a grid with 250 grid segments and a stretching factor of 1.03 is defined.

In order to allow comparison with the numerical results of Justesen (Justesen, 1991), the k-ε model (with friction velocity defined as $u_* = \sqrt{\left(\nu_t \left|\partial U/\partial z\right|\right)_{z=z_o}}$) will be applied in the

present numerical simulations. A fully implicit timestepping ($\theta = 1$) is applied during 20 cycles of duration $T_{cycle} = T$ and with a timestep of $\Delta t / T = 1/1440$.

Some numerical predictions are compared to the experimental data of Jensen et al. - i.e. the experimental data as processed by Justesen in (Justesen, 1991) - in the following figures:

- Profiles of turbulent mean velocity U in Figure 4-1 and Figure 4-2. Notice that the profiles are nondimensionalized by means of the freestream velocity amplitude U_o and bed roughness length k_n. The numerical results reproduce the features of the experimentally observed wave boundary layer, i.e. (i) the overshoot at zero freestream velocity, (ii) the distinct differences in shape in the acceleration and deceleration phases respectively, (iii) a logarithmic velocity distribution close to the wall.
- Bed friction velocity u_* as a function of time in Figure 4-3. Notice that the timeseries is nondimensionalyzed by means of U_o and the wave period T. The numerical prediction of the friction velocities seems quite accurate, which is advantageous for future modelling of sediment transport under influence of the considered oscillatory flow.
- Profile of turbulent kinetic energy averaged over a wave period, $<k>$, in Figure 4-4. . Notice that the profile is nondimensionalized by means of U_o and k_n. Notice that the numerical results underpredict the cycle-averaged k-levels.
- Profiles of turbulent kinetic energy k in Figure 4-5. . Notice that the profiles are nondimensionalized by means of U_o and k_n. While the numerical model calculates k directly, the experimental values for k are obtained indirectly from measured values of the normal Reynolds stresses, $k = 1.3\left(\overline{u'^2} + \overline{w'^2}\right)\Big/2$, based on an estimate for the third normal Reynolds stress, $\overline{v'^2}$. Notice that the numerical results underpredict the k-levels both near the wall as well as away from the wall.
- Profiles of the Reynolds stress $-\overline{u'w'}$ in Figure 4-6. . Notice that the profiles are nondimensionalized by means of U_o and k_n. While the experimental values are obtained directly from the measurements, the numerical values for the shear stress are obtained from the product of the calculated eddy viscosity and the gradient of the calculated mean velocity. Notice that the numerical predictions agree quite well with the experimental data.
- Profiles of the eddy viscosity ν_t in Figure 4-7. Notice that the profiles are nondimensionalized by means of U_o and k_n. While the numerical values are directly calculated by the $k-\varepsilon$ model, the experimental data are indirectly estimated (see Fig. 7 in (Justesen, 1991)), based on the ratio of the measured shear stresses and the gradient of the measured (and smoothed) mean velocities. There is a reasonable agreement, but clearly the numerical model gives a much smoother variation of the eddy viscosity than found from the experiments. One should point out, however, that the way the experimental values are estimated, is not reliable in those regions where the mean velocity is maximum (i.e. a zero gradient) and where at the same time the Reynolds shear stress is very small.

Notice that the numerical predictions of the present code have the same level of agreement with the experimental data as the numerical results of (Justesen, 1991).

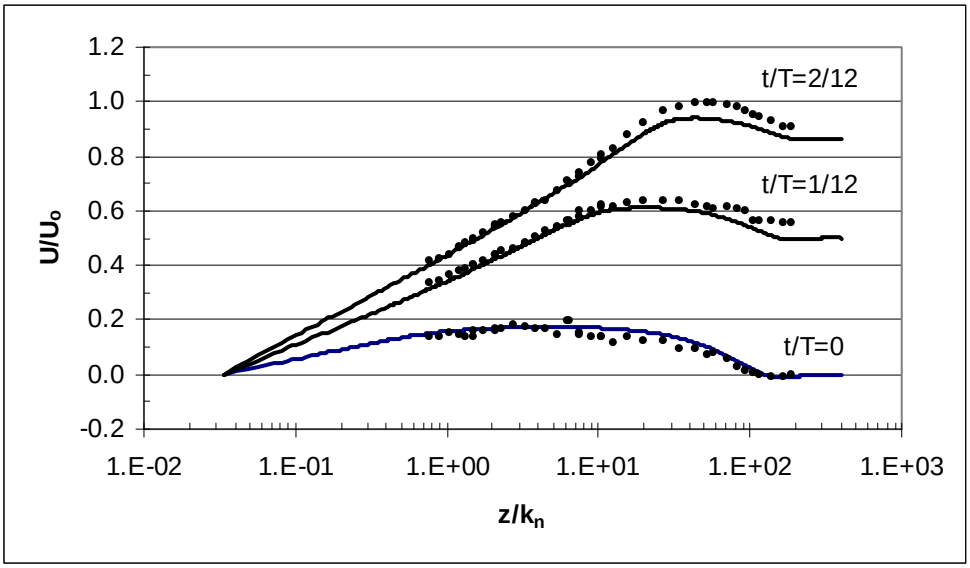

Figure 4-1 : Turbulent mean velocity profiles in the acceleration phase: numerical prediction (line) versus experimental data (dots)

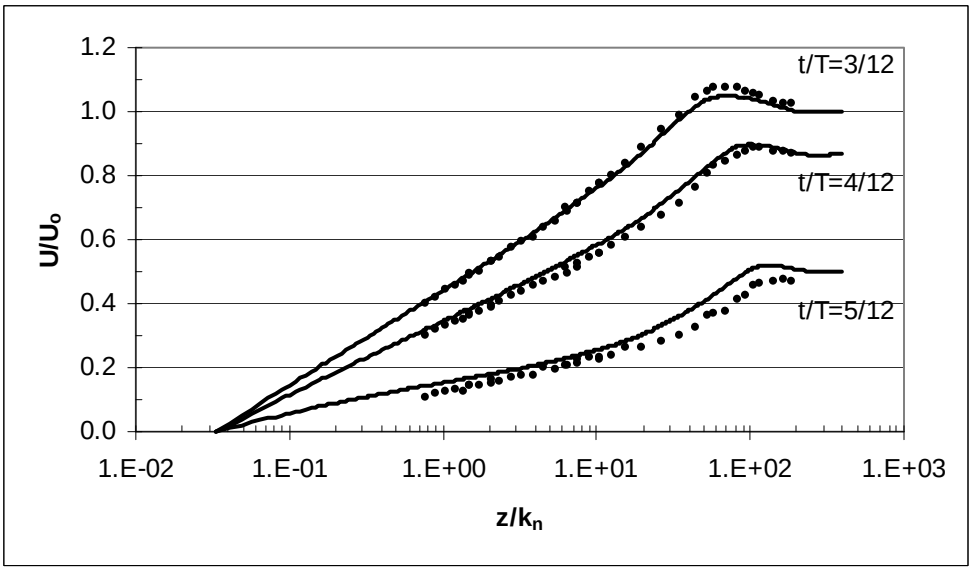

Figure 4-2 : Turbulent mean velocity profiles in the deceleration phase: numerical prediction (line) versus experimental data (dots)

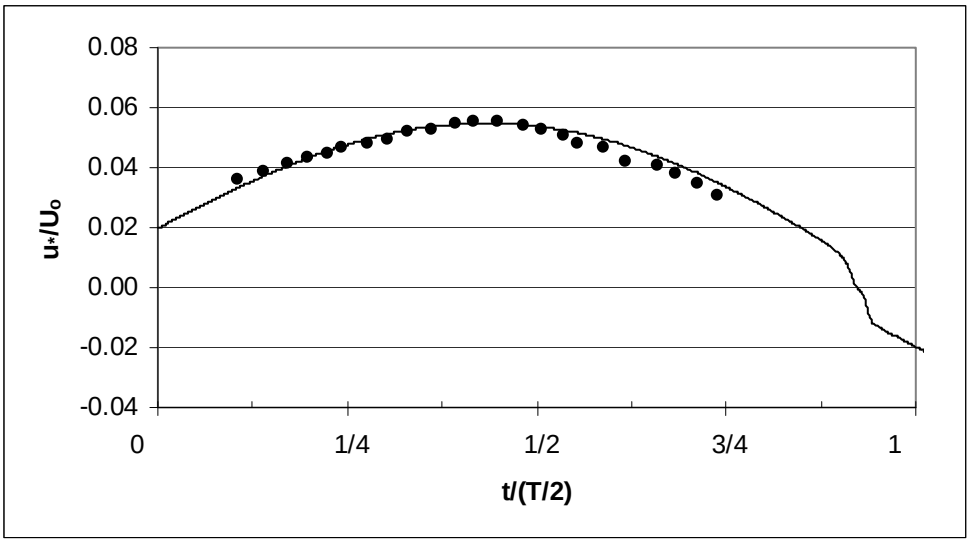

Figure 4-3 : Bed friction velocity u_* as a function of time : numerical prediction (line) versus experimental data (dots)

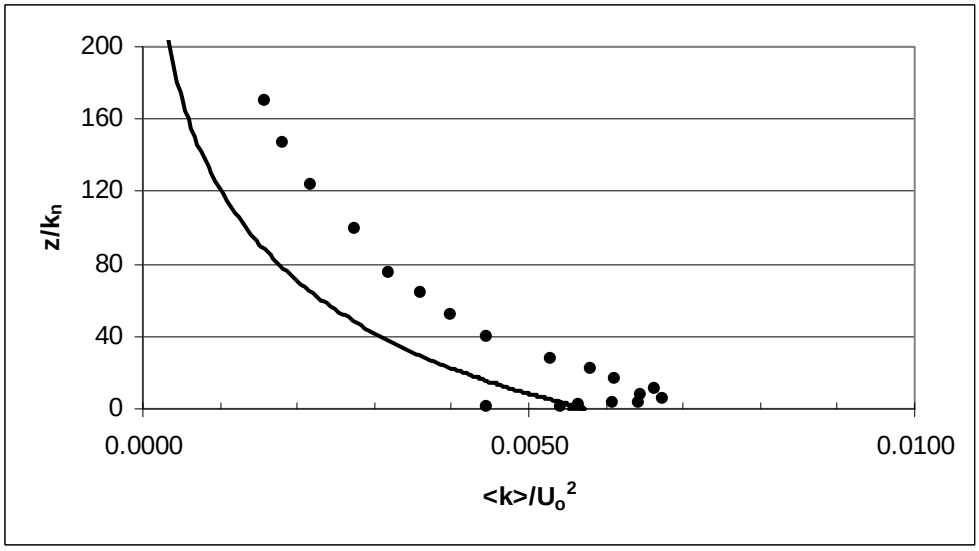

Figure 4-4 : Profile of turbulent kinetic energy averaged over a wave period, <*k*>: numerical prediction (line) versus experimental data (dots)

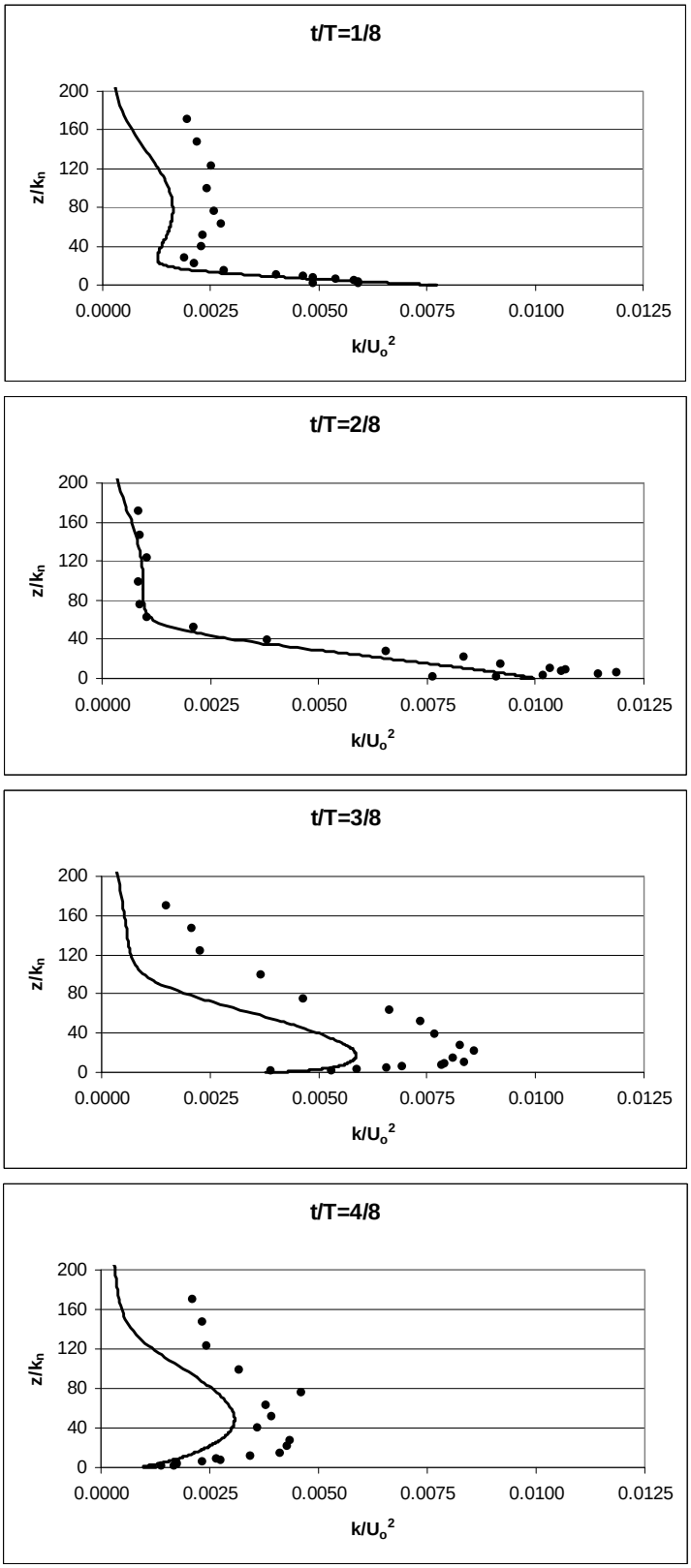

Figure 4-5 : Profiles of turbulent kinetic energy *k* : numerical prediction (line) versus experimental data (dots)

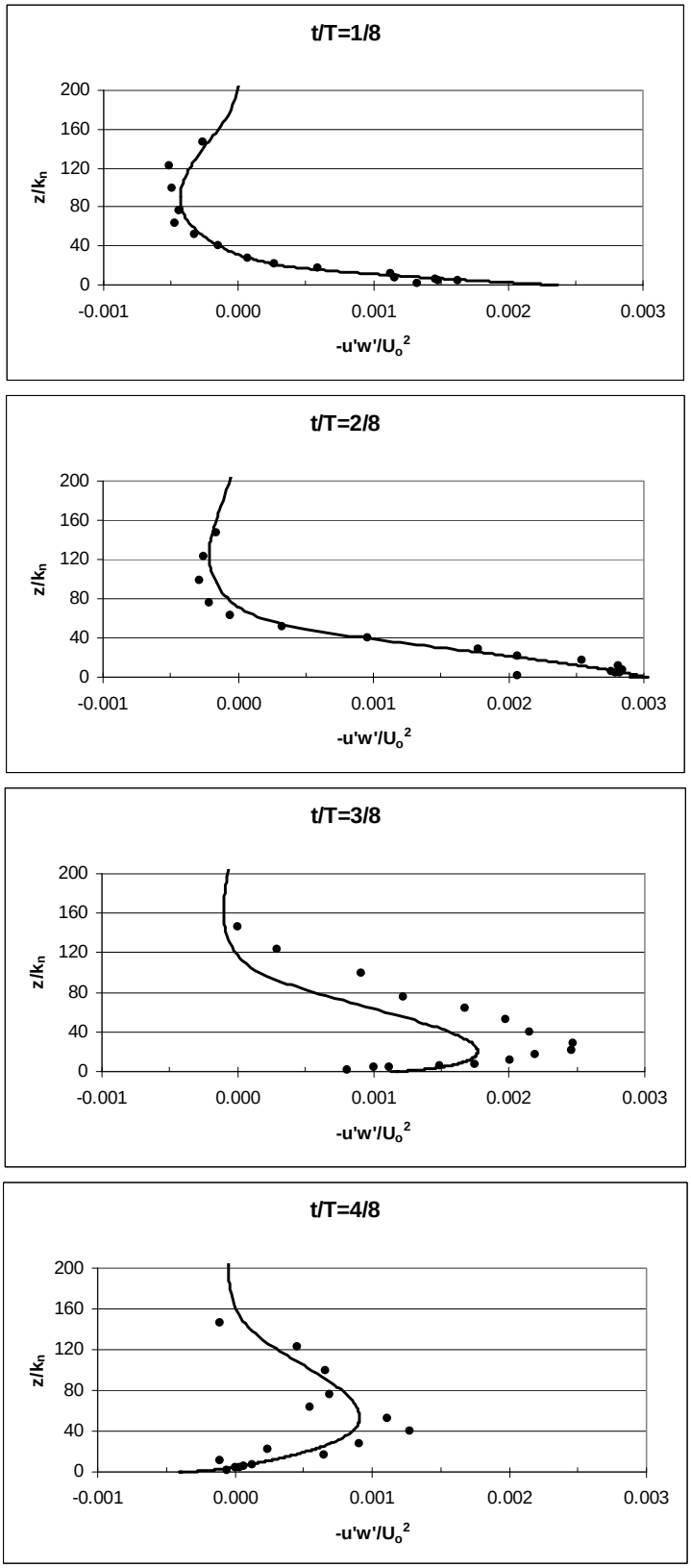

Figure 4-6 : Profiles of the Reynolds stress $-\overline{u'w'}$: numerical prediction (line) versus experimental data (dots)

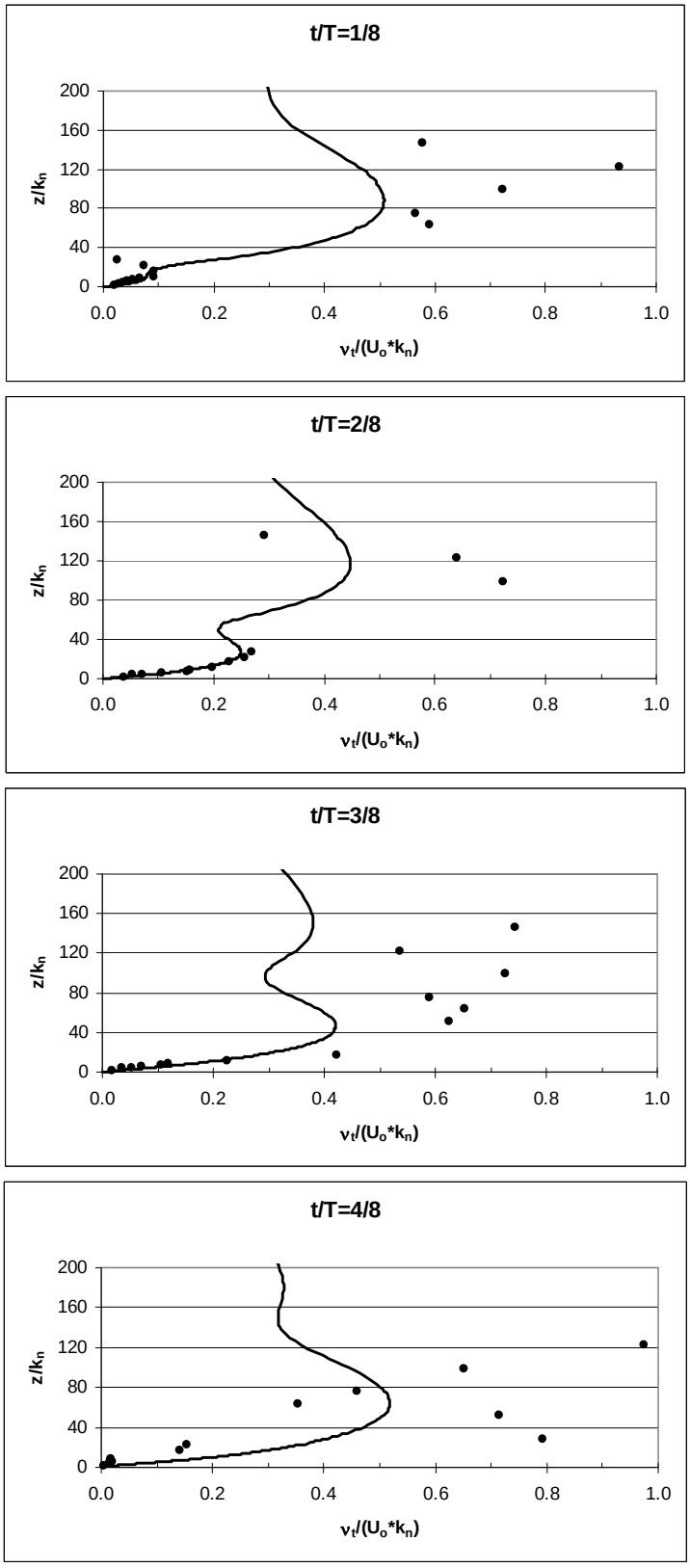

Figure 4-7: Profiles of the eddy viscosity ν_t : numerical prediction (line) versus experimental data (dots)

4.1.2 Asymmetric wave

Ribberink and Al-Salem (Al-Salem, 1993) investigated oscillatory boundary layers in asymmetric waves (on which a small current of 0.024 m/s is superimposed) through experiments in the Large Oscillating Wave Tunnel (LOWT) of Delft Hydraulics.

In this section experiment no. C1 will be considered, of which some characteristic flow parameters are given in Table 4-1:

- wave period T,
- crest velocity U_c, i.e. maximum horizontal velocity in the direction of wave propagation,
- trough velocity U_t, i.e. maximum horizontal velocity opposite to the direction of wave propagation,
- degree of wave asymmetry $R=U_c/(U_c+U_t)$,
- root-mean-square velocity U_{rms},
- time-averaged velocity $<U>$,
- third-order velocity moment $<U^3>$, i.e. time-averaged value of U^3.

	T	U_c	U_t	R	U_{rms}	$<U>$	$<U^3>$
	[s]	[m/s]	[m/s]	[-]	[m/s]	[m/s]	[m^3/s^3]
Exp. C1	6.5	1.11	0.58	0.66	0.59	0.024	0.124
Curve fit	6.5	1.04	0.56	0.65	0.59	0.024	0.129

Table 4-1 : Characteristic flow parameters of asymmetric wave

A timeseries of the measured horizontal velocity at a height of 0.257 m above the bed in experiment no. C1 is presented in Fig. 8.5 of (Al-Salem, 1993). A digitized version of this timeseries is also shown in Figure 4-8.

An analytical approximation of the following form,

$$U(t) = U_{mean} + U_1 \sin(\omega t + \varphi) - U_2 \cos(2(\omega t + \varphi))$$

i.e. a mean current plus a second order Stokes wave (in which $\omega=2\pi/T$), is derived through a curve fitting procedure (with MATLAB) applied to the measured timeseries. The parameters defining the curve fit are given in Table 4-2 . The curve fit is compared to the measured timeseries in Table 4-1 and Figure 4-8.

In the remainder of this section, the curve fit defined above will be used as the velocity boundary condition $U_\infty(t)$ imposed at the top of the domain, i.e. at z_∞=0.257m.

T	U_{mean}	U_1	U_2	φ
[s]	[m/s]	[m/s]	[m/s]	[rad]
6.5	0.024	0.7998	0.2181	0.1949

Table 4-2 : Parameters of analytical curve fit

In experiment C1 a sand bed was present with d_{50}=210 μm. Hence, a roughness height k_n of 525 μm (=2.5d_{50}) and a zero-velocity level z_o of 17.5 μm (=k_n/30) will be assumed.

In order to allow comparison with the numerical results of Al-Salem (Al-Salem, 1993), the mixing-length model will be applied in the present numerical simulations. The grid (between levels z_o and z_∞) is defined by means of 200 grid segments and a stretching factor of 1.05. A fully implicit timestepping ($\theta = 1$) is applied during 25 cycles of duration $T_{cycle} = T$ and with timestep $\Delta t / T = 1/1080$.

Some instantaneous flow velocity profiles are shown in Figure 4-9 and Figure 4-10. The numerical results are compared to experimental values obtained from Fig. 9.6 of (Al-Salem, 1993). Notice that the present numerical results compare well to the numerical solutions presented in Fig. 9.6 of (Al-Salem, 1993).

Analogously, Figure 4-11 presents a comparison between the net (i.e. averaged in time over a wave period) flow velocity profile calculated with the present model and the experimental profile obtained from Fig. 9.7 of (Al-Salem, 1993). Again, the present numerical result compares well to the numerical solution presented in Fig. 9.7 of (Al-Salem, 1993).

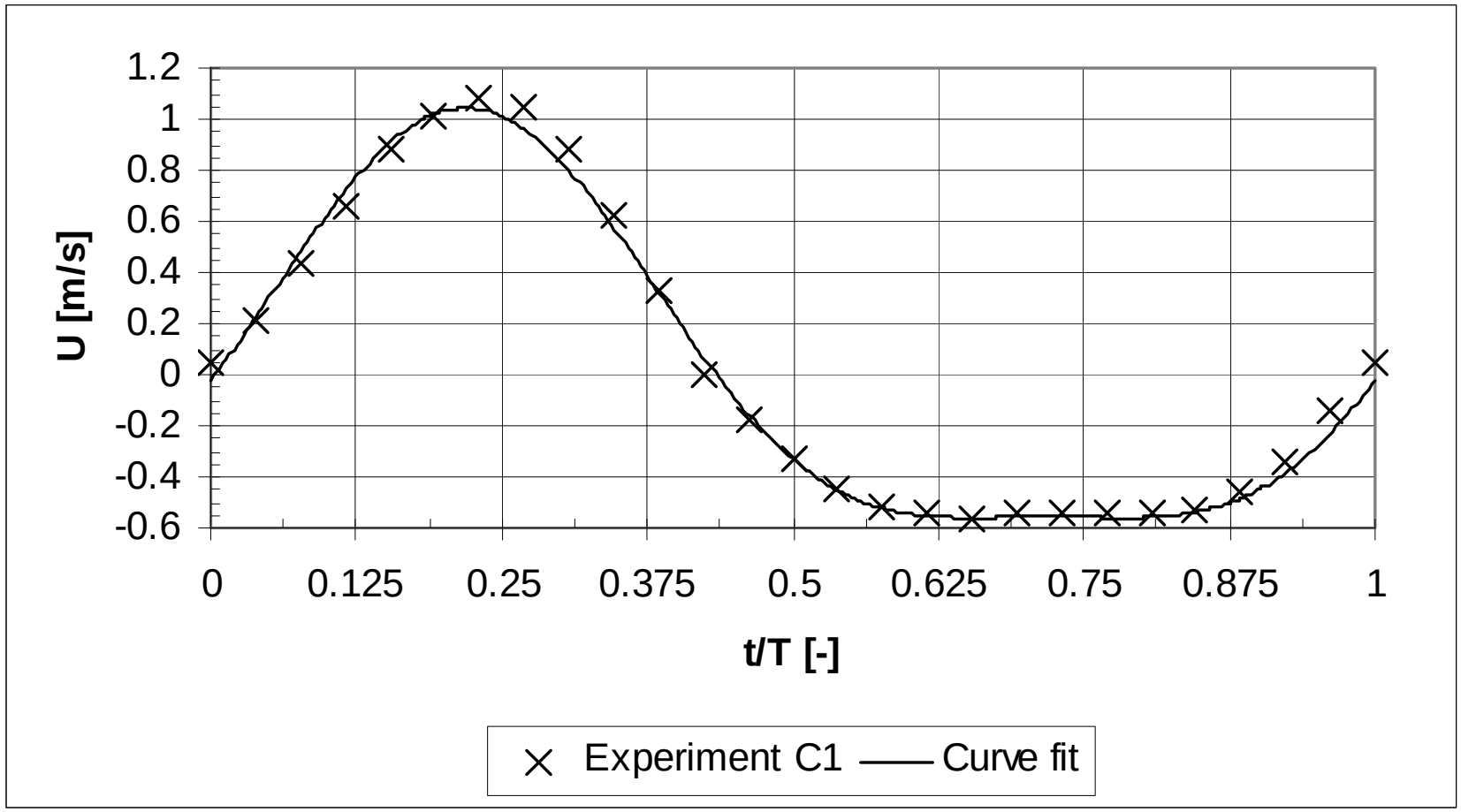

Figure 4-8 : Comparison of measured timeseries of horizontal velocity at Z=0.257 m (experiment C1 in Al-Salem, 1993) to analytical curve fit

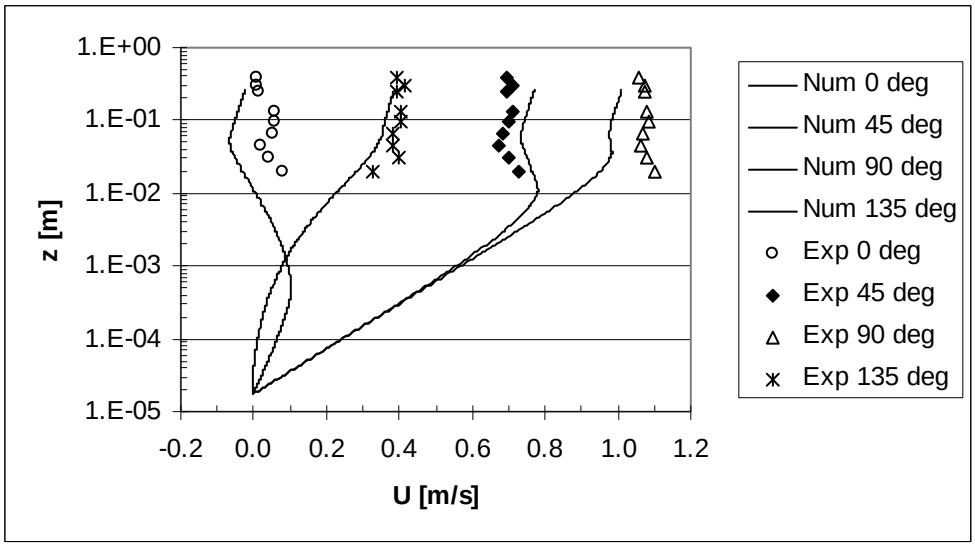

Figure 4-9 : Measured (Al-Salem 1993) and computed instantaneous flow velocity profiles

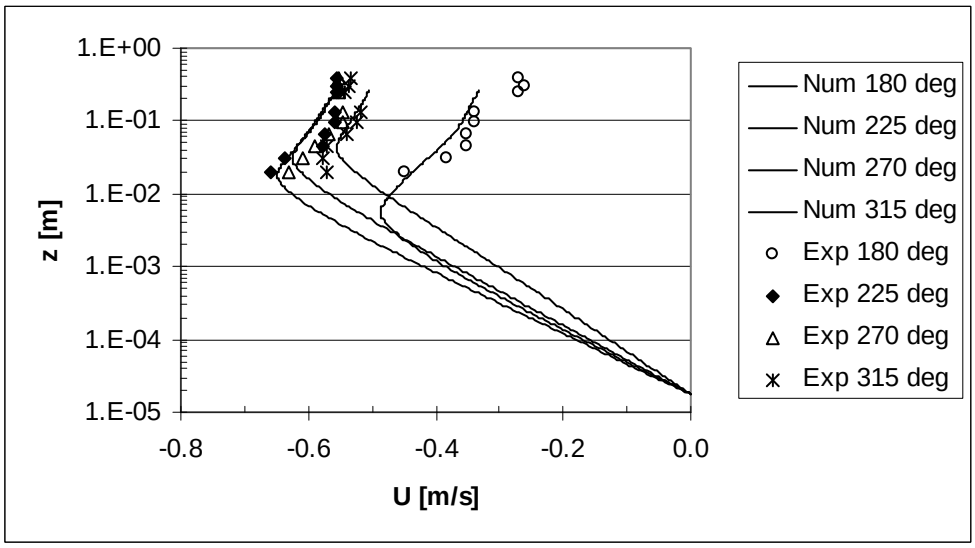

Figure 4-10 : Measured (Al-Salem 1993) and computed instantaneous flow velocity profiles

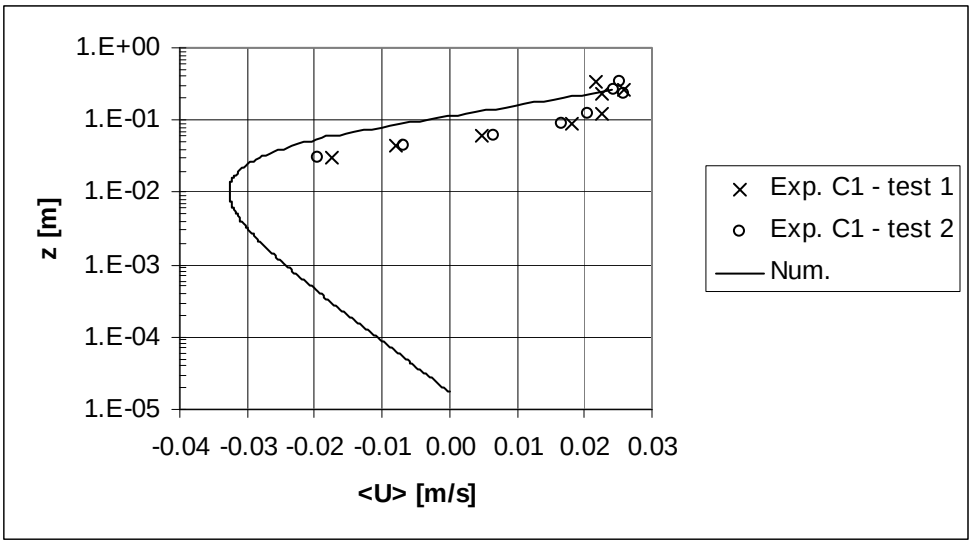

Figure 4-11 : Measured (Al-Salem 1993) and computed net flow velocity profiles

4.1.3 Wave group

Consider a wave group which is characterized by a free stream velocity oscillation of the following general form:

$$U_\infty(t) = U_o \sin\left(\frac{\omega t}{n}\right)\sin(\omega t)$$

in which :

- the first factor, U_o, is the maximum amplitude of the velocity ; the corresponding root-mean-square velocity is $U_{rms} = U_o / 2$,
- the second factor is the envelope wave, in which *n* represents the number of half waves in the group (of duration $nT/2$),
- the third factor is the fast oscillating wave with period *T* and angular frequency $\omega = 2\pi/T$.

Notice that the free stream velocity is periodic with a period *nT* (i.e. the duration of 2 groups). Therefore a numerical simulation of a wave group will be based on a timestepping procedure with consecutive cycles of duration $T_{cycle} = nT$, in order to obtain converged results.

Just to briefly sketch the capabilities of the present code, an example with *n=8* is given in Figure 4-12. In Figure 4-13, the bed friction velocities in case of the wave group (calculated with $k-\varepsilon$–model) are compared to those in case of a sinusoidal wave having the same root-mean-square velocity U_{rms}.

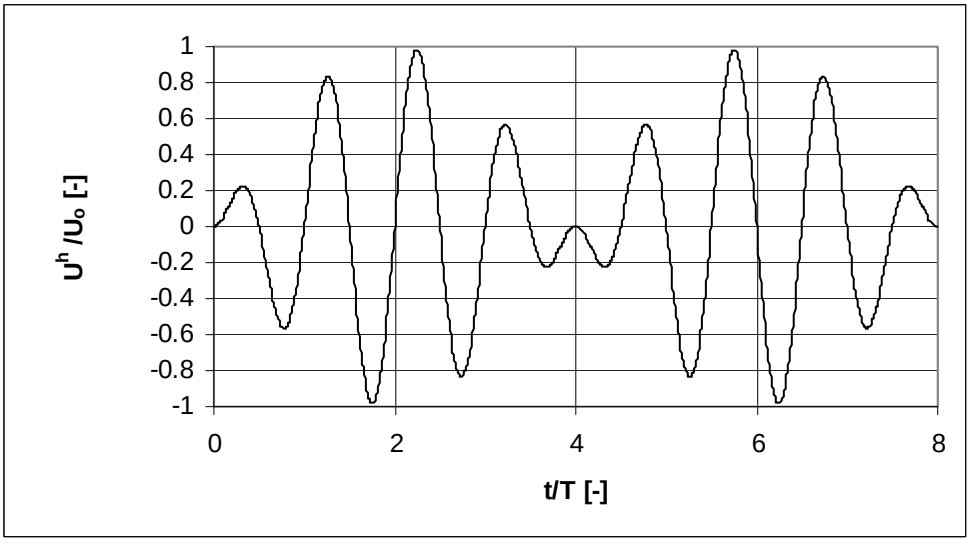

Figure 4-12 : Free stream velocity $U_\infty(t)$ in case of a wave group with 8 half-waves per group($n = 8$). Two consecutive groups are required for $U_\infty(t)$ to be periodic.

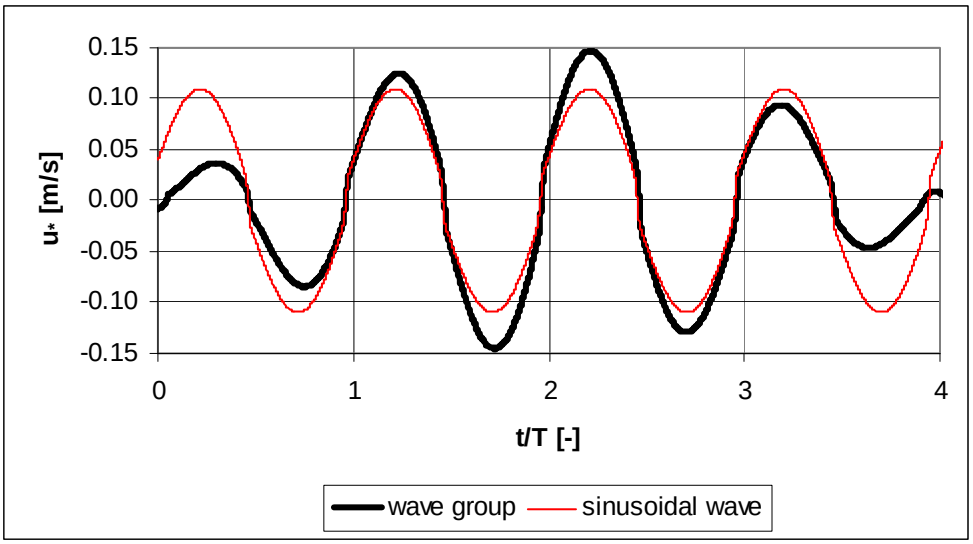

Figure 4-13 : Bed friction velocity as a function of time for a wave group (n=8) and for a sinusoidal wave, both having the same U_{rms}.

4.2 Steady current flow

Consider a steady, turbulent current driven by a pressure gradient

$$-\frac{1}{\rho}\frac{\partial p}{\partial x} = gS\,,$$

in which $S=1.402\ 10^{-5}$. The current flows over a plane bed with roughness $k_n = 0.005\ m$, hence $z_o = 1.67\ 10^{-4}\ m$. The flow depth is taken as $z_\infty = 10\ m$. Notice that this testcase is inspired by pages 79-81 in (Fredsøe, 1993).

This steady current flow will be simulated by means of the k-ε model (with friction velocity defined as $u_* = \sqrt{\left(\nu_t \left|\partial U/\partial z\right|\right)_{z=z_o}}$). The velocity boundary condition at the top of the domain is of the homogeneous Neumann type.

Between levels z_o and z_∞, 250 grid segments are defined with a stretching factor of 1.04.

Some results are shown in the following figures:

- the turbulent mean velocity *(U)* profile in Figure 4-14 ; notice that the profile has a logarithmic shape,
- the Reynolds stress ($-\overline{u'w'}$) profile in Figure 4-15,
- the profile of the turbulent kinetic energy *(k)* in Figure 4-16 ; notice that k is nearly constant near the wall (which is in accordance with the boundary condition and the assumption of a constant shear stress layer: $k(z_o) = u_*^2 \Big/ \sqrt{c_\mu} \Rightarrow \partial k/\partial z = 0$),
- the profile of the dissipation rate (ε) of the turbulent kinetic energy in Figure 4-17 ; notice that ε achieves large values near the wall (which is in accordance with the boundary condition $\varepsilon(z_o) = u_*^3 \Big/ \kappa z_o$),
- the eddy viscosity (ν_t) profile in Figure 4-18.

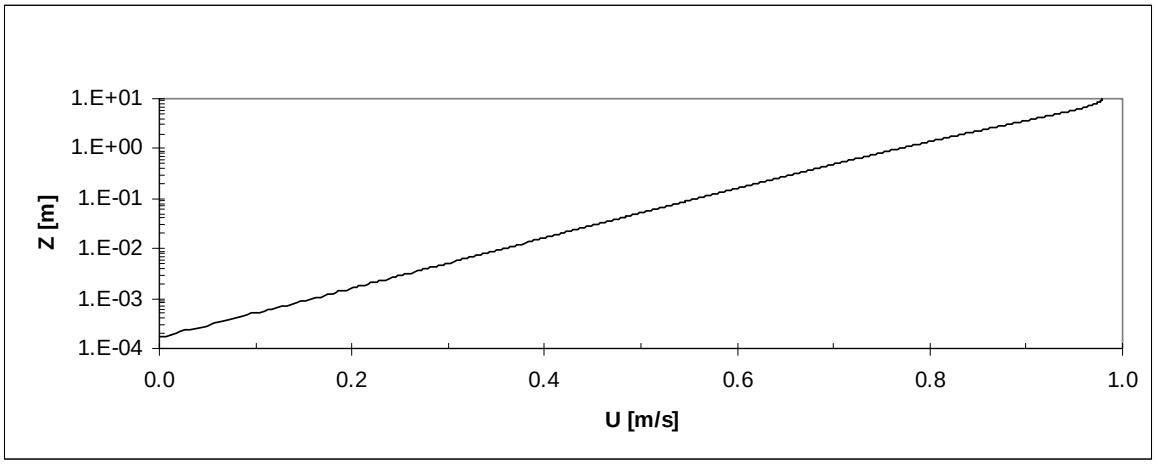

Figure 4-14 : Turbulent mean velocity profile in steady current flow

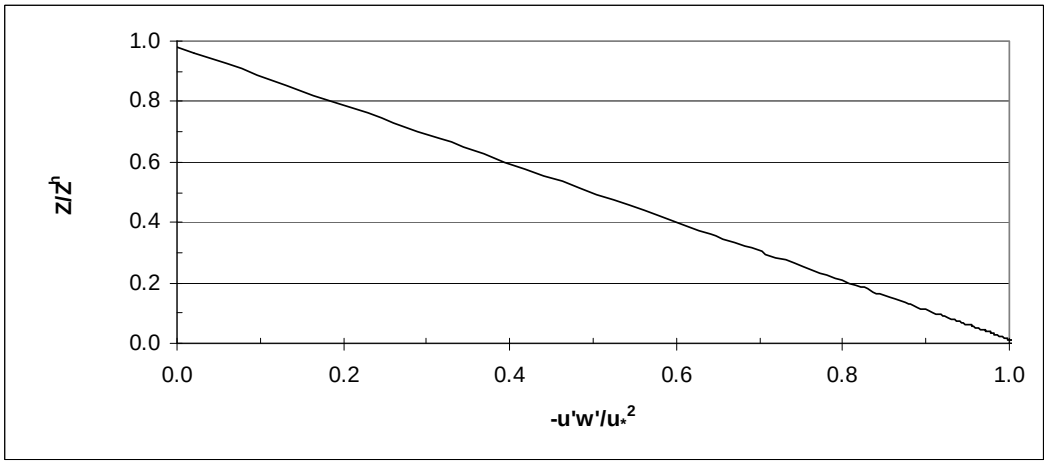

Figure 4-15 : Reynolds stress profile in steady current flow

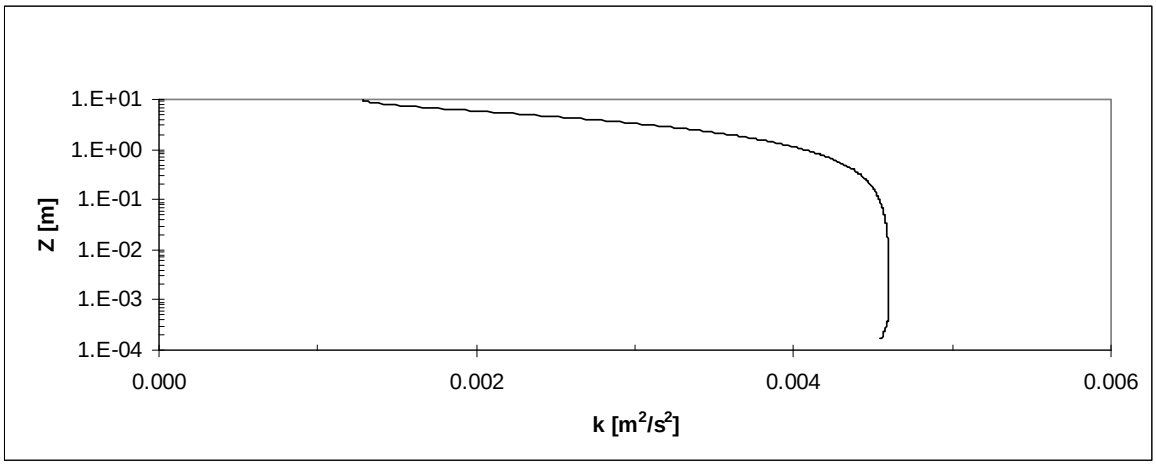

Figure 4-16 : Profile of turbulent kinetic energy in steady current flow

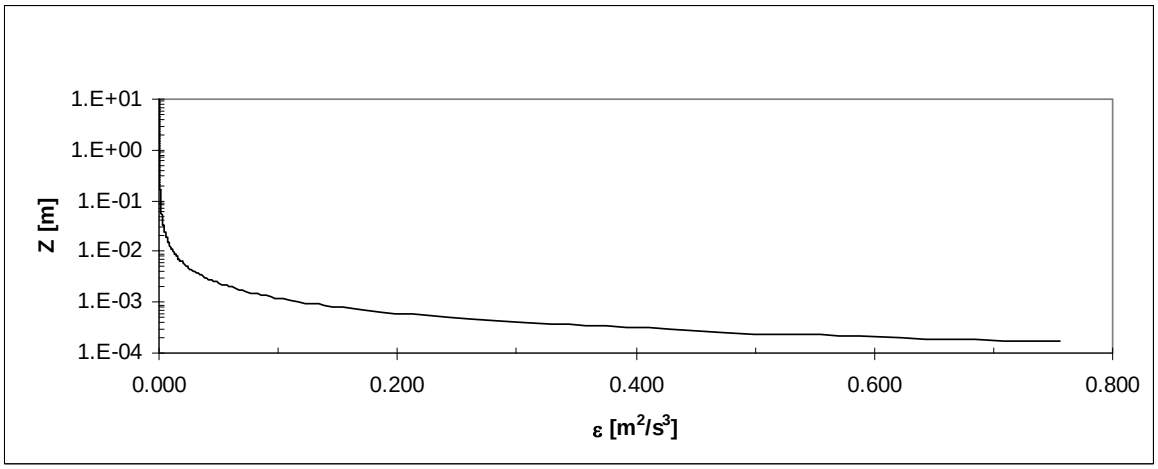

Figure 4-17 : Profile of dissipation rate of turbulent kinetic energy in steady current flow

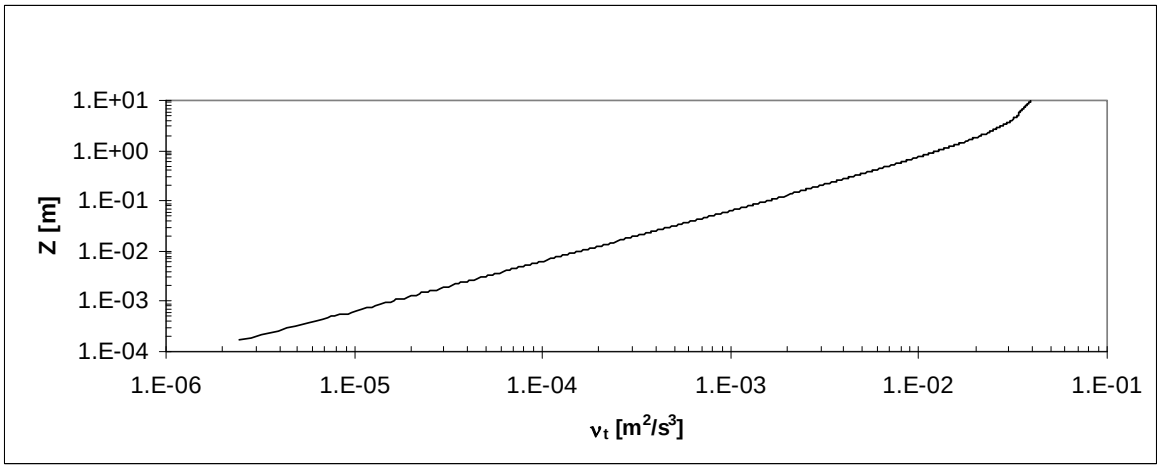

Figure 4-18 : Eddy viscosity profile in steady current flow

4.3 Combined current and oscillatory flow

Consider the same steady current flow testcase as defined in section 4.2:

- a pressure gradient given by $S=1.402\ 10^{-5}$,
- a plane bed with roughness $k_n=0.005\ m$, hence $z_o=1.67\ 10^{-4}\ m$,
- a flow depth of $z_\infty=10\ m$.

The corresponding freestream current speed is about $U_{\infty c}$=0.98 m/s.

In this section, however, a (colinear) oscillatory flow will be superimposed on the aforementioned current. The oscillating flow is of the form:

$$U_\infty(t)=U_o\ \sin(\omega t),$$

in which U_o is the freestream velocity amplitude and $\omega=2\pi/T$ is the angular frequency. Recall that the combined current and oscillatory flow will be simulated by imposing the following pressure gradient:

$$-\frac{1}{\rho}\frac{\partial p}{\partial x}=\frac{\partial U_\infty}{\partial t}+gS\,.$$

A wave period of $T=7s$ is assumed. Three freestream velocity amplitudes, U_o, will be considered: 0.5, 1.0 and 1.5 m/s. For the sake of comparison, the results of the steady current case (i.e. corresponding to U_o=0.0 m/s) will also be shown in the figures below.

Notice that these combined flow testcases are inspired by pages 79-81 in (Fredsøe, 1993), where some numerical results of (Davies et al., 1988) are presented.

To simulate the combined flow testcases numerically with the present code, the same turbulence model (k-ε), the same velocity boundary condition at the top of the domain (homogeneous Neumann type) and the same grid (250 segments, stretching factor 1.04) as in section 4.2 will be adopted.

First some detailed instantaneous profiles will be presented for the particular combined flow testcase with U_o=1.0 m/s, in order to illustrate one of the advantages of the $k-\varepsilon$ model, i.e. being able to predict the turbulence characteristics as a function of space and time:

- turbulent mean velocity profiles during the deceleration phase in Figure 4-19,
- turbulent mean velocity profiles during the acceleration phase in Figure 4-20,
- profiles of the turbulent kinetic energy during the deceleration phase in Figure 4-21,
- profiles of the dissipation rate of turbulent kinetic energy during the deceleration phase in Figure 4-22,
- profiles of the eddy viscosity during the deceleration phase in Figure 4-23.

Notice that the present results compare well to the numerical results of (Davies et aL., 1988) presented in (Fredsøe, 1993).

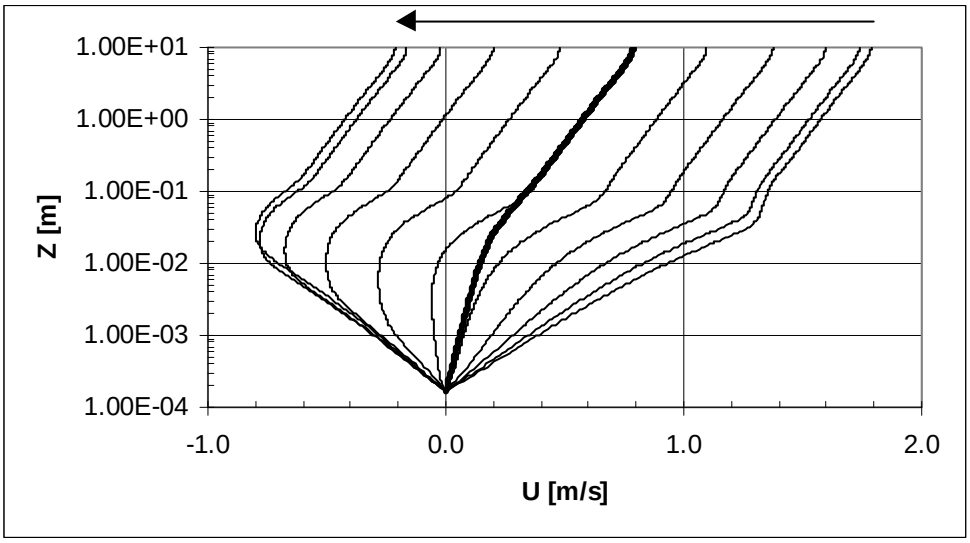

Figure 4-19 : Instantaneous velocity profiles (phase interval 0.1π) during deceleration phase of combined current and oscillatory flow (U_o=1.0m/s). Time-averaged profile indicated in bold line.

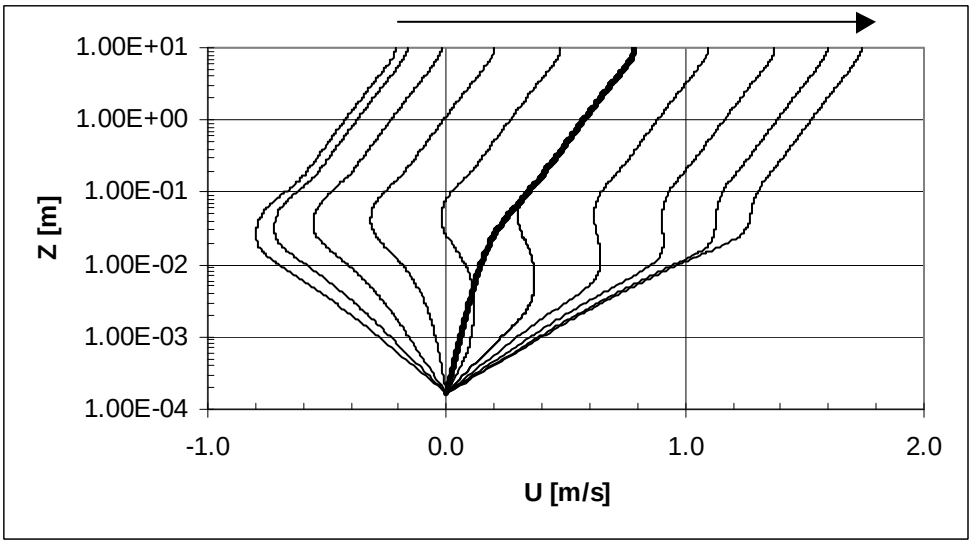

Figure 4-20 : Instantaneous velocity profiles (phase interval 0.1π) during acceleration phase of combined current and oscillatory flow (U_o=1.0m/s). Time-averaged profile indicated in bold line.

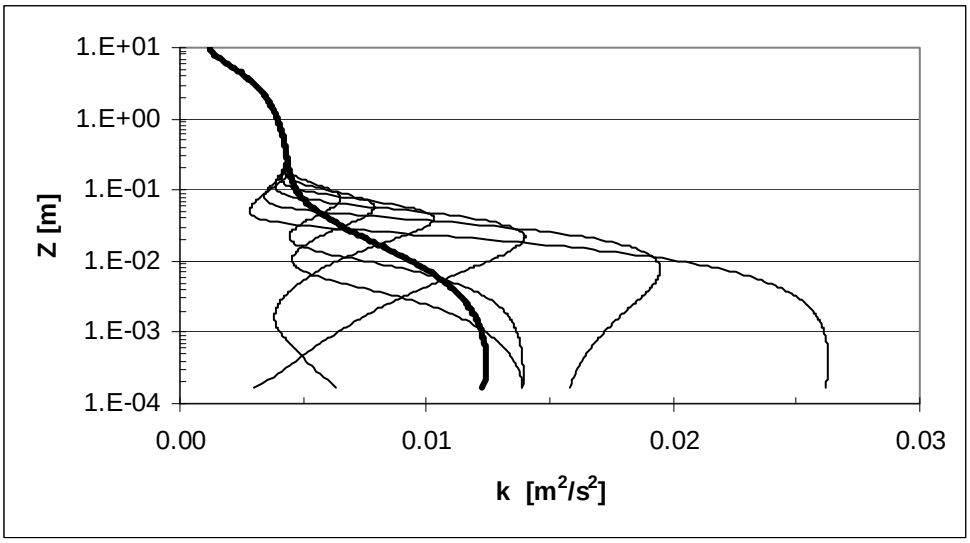

Figure 4-21 : Instantaneous profiles (phase interval 0.2π) of turbulent kinetic energy during deceleration phase of combined current and oscillatory flow (U_o=1.0m/s). Time-averaged profile indicated in bold line.

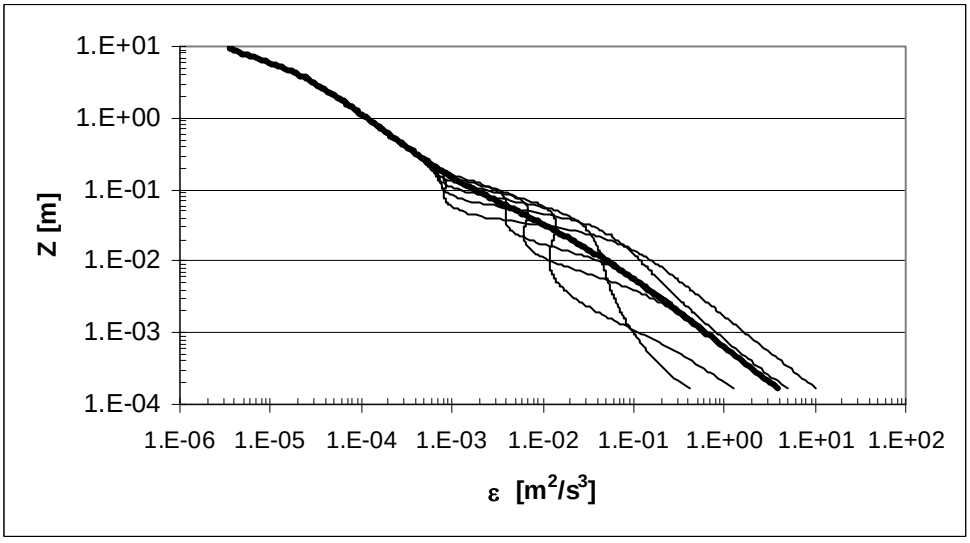

Figure 4-22 : Instantaneous profiles(phase interval 0.2π) of dissipation rate of turbulent kinetic energy during deceleration phase of combined current and oscillatory flow (U_o=1.0m/s). Time-averaged profile indicated in bold line.

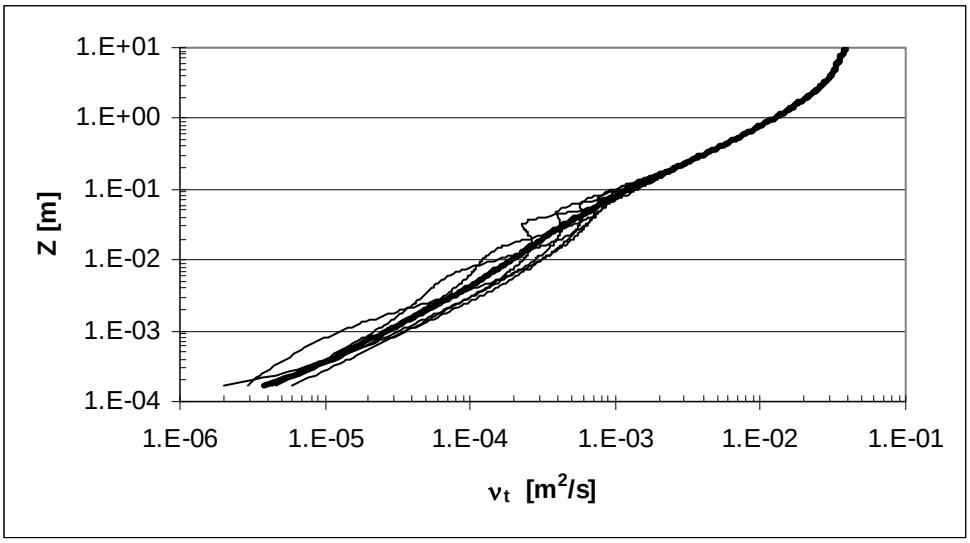

Figure 4-23 : Instantaneous profiles (phase interval 0.2π) of eddy viscosity during deceleration phase of combined current and oscillatory flow (U_o=1.0m/s). Time-averaged profile indicated in bold line.

The time-averaged (i.e. averaged in time over a wave period *T*) turbulent mean velocity profiles corresponding to the various combined current and oscillatory flows are given in Figure 4-24. Recall that the mean pressure gradient ($\propto S$) has been kept constant, while the near-bed wave-induced orbital motion (U_o) has been given different strengths in Figure 4-24, thereby giving rise to different flow resistances for the current. Hence, the mean flow velocity decreases with increasing values of U_o.

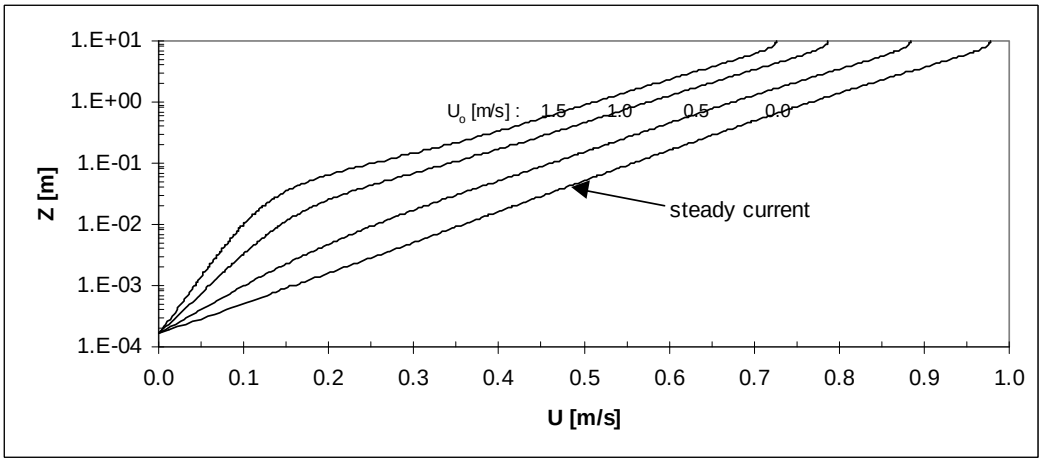

Figure 4-24 : Time-averaged velocity profiles for combined current and oscillatory flows

It can also be seen from the mean velocity profiles in Figure 4-24 that an inner and an outer logarithmic layer exist, the inner layer being associated to the wave boundary layer, while the outer layer corresponds to the current boundary layer.

Whereas the current boundary layer in a steady current ($U_o = 0$) can be described by

$$\frac{U(z)}{u_*} = \frac{1}{\kappa} \ln\left(\frac{z}{z_o}\right),$$

in which the zero-reference level z_o is a function of the wall roughness ($z_o = k_n/30$), superposition of an oscillating flow ($U_o \neq 0$) requires the net current above the wave boundary layer to be described by

$$\frac{U(z)}{u_*} = \frac{1}{\kappa} \ln\left(\frac{z}{z_A}\right),$$

in which z_A determines the so-called apparent roughness height $k_A (= 30.z_A)$ resulting from the wave-current interaction (see Figure 4-25). In other words, the flow above the wave boundary layer appears to feel a larger roughness, due to the presence of the waves.

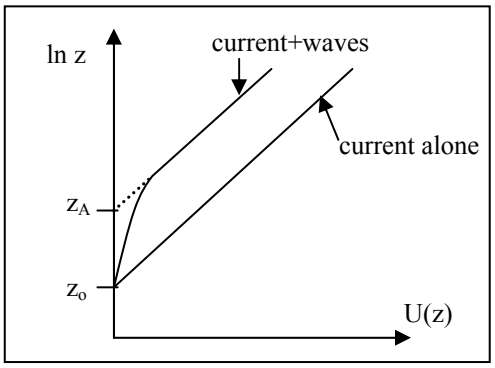

Figure 4-25 : Apparent roughness due to wave-current interaction

5 SUMMARY AND PROSPECTS

In this report, a **1DV hydrodynamic model** has been presented which describes the turbulent boundary layer flow over **plane and hydraulically rough beds** under the influence of combined **(colinear) oscillatory and current flows** in the freestream above the boundary layer. Under not too strict conditions (see section 1), oscillatory flows can be considered to be a good approximation for the near-bed flow under surface waves (which are common in coastal environments).

The **numerical approach** to solve the governing equations and boundary conditions has been carefully described, including some turbulence modelling aspects related to the **mixing-length model and the $k-\varepsilon$ model**. It is hoped that the presented material will serve as a **comprehensive introduction** to people who are less familiar with those topics which are often not extensively treated in basic courses on hydrodynamics and fluid mechanics.

Based on the described hydrodynamic model and numerical approach, a **computer code** has been developed, which allows to study several aspects of (interacting) wave and current boundary layers **without excessive computational costs**.

Some testcases have been presented, in order to provide a first testing of the code through comparison of the numerical predictions with published experimental and/or numerical data. The agreement between the present results and the published data is satisfactory. Other testcases have been merely presented to give an overview of the capabilities of the code. It is clear that more intensive application of the code would be interesting to further analyse issues such as selection of timestep and convergence monitoring.

As such, the developed computer code could serve as a **didactical tool** with which **students** become familiar to several aspects of (rough turbulent as well as laminar) wave and current boundary layers.

Moreover, the developed code can be used as a **'numerical laboratory'** to do **research** on waves and wave-current-interaction in the rough turbulent regime (as well as in the laminar regime):

- e.g. through comparison of the present numerical predictions with available experimental data (e.g. work of K. Trouw),
- or through comparison to numerical predictions made by others (e.g. work of K. Trouw),
- or through comparison to numerical predictions made with more simplified models (e.g. comparison of $k-\varepsilon$ model to Prandtl's mixing-length model ; comparison of $k-\varepsilon$ model to time-invariant eddy viscosity models like (Christofferson and Jonsson, 1985); comparison of $k-\varepsilon$ model to integrated momentum method)

on topics such as:

- **thickness** of a wave boundary layer (e.g. as a function of the amplitude to roughness ratio, A/k_n),

- instantaneous or time-averaged (over (half) period) **bottom friction** of waves (e.g. comparison to analytical formula),
- **phase difference** between bed shear stress and the freestream velocity,
- **energy dissipation** of waves,
- mean current velocity profile, **apparent roughness**, bottom friction and energy dissipation in waves-plus-current,
- intercomparison of **waves of different shape** (symmetric wave, asymmetric wave, wave group, broke wave, etc.) having the same root-mean-square freestream velocity,
- etc.

The present 1DV model forming the basis of the developed computer code, only deals with the hydrodynamics in waves and combined waves-current flows. If **an extra 1DV transport equation for the concentration of suspended sediments** (supplemented with a proper boundary condition for the bed concentration) were added, one could also model sand transport under influence of the aforementioned types of flow. See e.g. (Savioli and Justesen, 1997), where in a first approximation concentrations are considered to be low, allowing the particle-particle and particle-fluid interactions to be neglected. Under these assumptions one could simulate sand transport over **plane beds** (eventually covered with **small ripples**), excluding the sheet transport regime (i.e. high-shear conditions under which ripples are washed out and sediment transport takes place in a thin sheet at the bed).

In order to simulate **sheet flow**, additional modifications to the present code would be necessary, like e.g. accounting for a concentration-dependent fluid density in the momentum equation, introducing particle-particle and particle-fluid interactions terms [see e.g. (Toorman, 2000c;Toorman, 2000b;Toorman, 2000a) for a thorough investigation of the latter effects] in the turbulence model and modifying the boundary conditions for the concentration transport model. See e.g. (Li and Davies, 1996).

Finally, it is worth mentioning that simulation of sediment transport over beds with pronounced ripples requires at least a two-dimensional vertical (2DV) model [such as e.g. FENST2D (Toorman, 1997)] in order to capture the effects of flow separation and vortex formation upon sediment transport. Consequently, the present 1DV model is not suited to simulate such kind of flows. However, the present 1DV code could serve as a (computationally cheap) **testbench** during the early development and testing phase of a (more complex and computationally more expensive) **2DV** computer model, in the sense that predictions of the 2DV model for a testcase with 1DV and plane bed conditions can be compared to the predictions of the present 1DV model.

APPENDIX A. HIGH-RE VS. LOW-RE FORMULATIONS

In the present work, the effects of the molecular viscosity in the momentum equation

$$\frac{\partial U}{\partial t} = -\frac{1}{\rho}\frac{\partial p}{\partial x} + \frac{\partial}{\partial z}\left[\left(\nu + \nu_t\right)\frac{\partial U}{\partial z}\right],$$

are considered to be negligible as compared to the turbulent viscosity effects, i.e. the momentum equation is used in reduced form:

$$\frac{\partial U}{\partial t} = -\frac{1}{\rho}\frac{\partial p}{\partial x} + \frac{\partial}{\partial z}\left(\nu_t \frac{\partial U}{\partial z}\right).$$

This simplification is acceptable since the present work focuses on flow over hydraulically rough beds, where the near-wall flow will be dominated by flow separation at the roughness elements on the wall (see also APPENDIX C).

Also in the transport equations for k and ε,

$$\frac{\partial k}{\partial t} = \frac{\partial}{\partial z}\left[\left(\frac{\nu_t}{\sigma_k}\right)\frac{\partial k}{\partial z}\right] + P - \varepsilon\,,$$

$$\frac{\partial \varepsilon}{\partial t} = \frac{\partial}{\partial z}\left[\left(\frac{\nu_t}{\sigma_\varepsilon}\right)\frac{\partial \varepsilon}{\partial z}\right] + c_{\varepsilon 1}\frac{\varepsilon}{k}P - c_{\varepsilon 2}\frac{\varepsilon^2}{k}\,,$$

the molecular viscosity terms are absent. This form of the transport equations is usually referred to as the 'high-Reynolds-number formulation'.

Note that this formulation is no longer valid if ν_t/ν is smaller than about 10, i.e. if viscous effects become important. In order to apply the k-ε model in areas where viscous effects are important - like e.g. in the viscous sublayer close to a hydraulically smooth bed, see APPENDIX C - two classical remedies are available:

- Modify the transport equations to make them also valid for regions where the turbulence level is low, hence the name of 'low-Reynolds-number models'. For wall bounded flows e.g., this requires very fine grids in order to resolve the sharp gradients (of the tangential velocity, k and ε) in the near-wall viscous sublayer. For further information on low-Re formulations, the reader is referred to e.g. (Rodi, 1984) and (Gatski, 1996).
- Solve the transport equations in high-Reynolds-number formulation only in the region of developed turbulence and bridge over to the wall with the help of some empirical 'wall function' (see also APPENDIX E and APPENDIX F). This approach allows to minimize the number of grid points in the direction normal to the wall, and thus save computer time and memory.

REMARK: *In order to be able to simulate also laminar flows with the present code (for didactical purposes), the momentum equation has been programmed with a total viscosity of the following form:*

$$Flag.\nu + (1 - Flag).\nu_t ,$$

in which the flag is put to 0 in case of turbulent flows, whereas the flag gets a value of 1 in case of laminar flows.

APPENDIX B. PRESSURE GRADIENT DRIVING A STEADY CURRENT

A steady, uniform, turbulent current is defined by imposing the following pressure gradient term in the momentum equation:

$$-\frac{1}{\rho}\frac{\partial p}{\partial x} = gS\,,$$

in which g is the gravitational acceleration and S is the slope of the energy line.

Usually, one wants to simulate a steady current with a given freestream current speed $U_{\infty c}$ (at z=z_∞). Therefore, a relationship between $U_{\infty c}$ and S is required.

An (approximate) relationship can be derived based upon the following equations:

- the assumption of a logarithmic velocity profile, being valid up to $z = z_\infty$: $U_{\infty c} = \frac{u_*}{\kappa}\ln\left(\frac{z_\infty}{z_o}\right)$,
- the definition of the friction velocity: $u_* = \sqrt{\tau_w/\rho}$,
- a force balance : $\tau_w = -(z_\infty - z_o)\frac{\partial p}{\partial x}$ [notice that a shearless freestream has been assumed at $z = z_\infty$],
- the definition of the pressure gradient term: $-\frac{1}{\rho}\frac{\partial p}{\partial x} = gS$,

from which one can derive the requested relationship:

$$S = \frac{1}{g(z_\infty - z_o)}\left[\frac{\kappa U_{\infty c}}{\ln(z_\infty/z_o)}\right]^2.$$

Notice that the foregoing relation is no longer valid if an oscillatory flow is superimposed upon the current, since the wave boundary layer is felt by the current as an increased (so-called apparent) roughness. In that case, the relation

$$U_{\infty c} = \frac{u_*}{\kappa}\ln\left(\frac{z_\infty}{z_o}\right),$$

which follows from the assumed logarithmic velocity profile with roughness height z_o based upon the sediment grain size ($z_o = k_n/30 = d_{50}/12$), is no longer appropriate to describe the turbulent mean velocity profile of the current. See section 4.3 and e.g. chapter 3 in (Fredsøe, 1993)

APPENDIX C. HYDRAULICALLY ROUGH VS. SMOOTH WALL

Consider the turbulent flow over a plane wall characterized by roughness elements with a characteristic roughness height, k_n. The wall roughness depends on the shape, the density and the mobility of the roughness elements. Often the wall roughness is expressed by means of an equivalent sand roughness, following the experiments of Nikuradse (1932) with rough surfaces consisting of glued uniform sand particles.

In a turbulent flow over a plane wall, a near-wall viscous sublayer might be present, in which turbulent shear stresses become negligible with respect to the stresses due to molecular diffusion. The thickness of the viscous sublayer, δ, is of the order of ν/u_*, in which ν is the molecular viscosity and $u_* = \sqrt{\tau_w/\rho}$ the wall friction velocity.

Depending on the relative magnitude of k_n with respect to δ, two types of beds are usually distinguished:

- a hydraulically rough wall ($k_n >> \delta$),
- a hydraulically smooth bed ($k_n << \delta$).

In turbulent flow over a hydraulically rough wall, the roughness elements extend through the viscous sublayer. Consequently, the near-wall flow is dominated by flow separation at the roughness elements. Hence, viscous effects are negligible, i.e. one can no longer distinguish a viscous sublayer,

In turbulent flow over a hydraulically smooth wall, on the other hand, the roughness elements are hidden away in the viscous sublayer. Consequently, the roughness elements are too small to influence the velocities in the fully turbulent region above the viscous sublayer.

The aforementioned experiments of Nikuradse have shown that the velocity profile in the fully turbulent region of a steady turbulent flow over a plane bed, can be expressed as follows:

$$\frac{U(z)}{u_*} = \frac{1}{\kappa}\ln\left(\frac{z}{z_o}\right),$$

in which the equivalent roughness length, z_o, is given by $z_o = k_n/30$ in case of hydraulically rough flow. Notice that z_o represents the zero-velocity reference level, since $U(z_o) = 0$, and that z_o depends on the wall roughness (and not on the fluid viscosity).

For a hydraulically smooth wall, on the other hand, the equivalent roughness length, z_o, should be taken as $z_o = \frac{\nu}{Eu_*}$, in which the smooth wall roughness parameter $E \approx 9 \pm 2$. Notice that z_o depends on the fluid viscosity (and not on the wall roughness).

For more details, the reader is referred to the literature on turbulent wall boundary layers, see e.g. most handbooks on fluid mechanics.

APPENDIX D. DIRICHLET VS. NEUMANN TYPE BOUNDARY CONDITIONS

In the literature on partial differential equations (PDE) and their numerical solution, a distinction is often made between different types of boundary conditions.

Be φ the variable (e.g. U, k or ε) for which a time-dependent PDE is solved along a z-axis. Hence, φ is a function z and t, which can be denoted as follows: $\varphi(z,t)$. Be z=z_b the position of the point at which a boundary condition has to be applied at each instant t.

- A so-called Dirichlet type boundary condition can then be written as follows:

$$\varphi(z = z_b, t) = c,$$

in which c is a given (possibly time-dependent) value. In other words, the variable φ itself gets a fixed, known value at the considered boundary point z=z_b. In case the given constant is zero, $c = 0,$ the foregoing boundary condition is said to be of the homogeneous Dirichlet type.

- A so-called Neumann type boundary condition can be written as follows:

$$\left(\frac{\partial \varphi}{\partial z}\right)_{z=z_b,t} = c,$$

in which c is a given (possibly time-dependent) constant. In other words, the gradient of the variable φ gets a fixed, known value at the considered boundary point z=z_b. In case the given constant is zero, $c = 0,$ the foregoing boundary condition is said to be of the homogeneous Neumann type.

APPENDIX E. VELOCITY BOUNDARY CONDITIONS AT THE BED

For the turbulent flow over a hydraulically rough, plane bed, a velocity boundary condition at the bed is suggested by the theoretical considerations and Nikuradse's experiments (for a steady current) which are briefly described in APPENDIX C, i.e. one can apply a no-slip condition at the zero-velocity reference level:

$$U(z_o, t) = 0 \text{ at } z = z_o = k_n/30 .$$

According to (Justesen, 1991), this boundary condition can safely be applied for oscillatory flows over rough beds if the amplitude to roughness ratio A/k_n exceeds a value of about 30. Otherwise, the boundary condition makes no sense and the flow around each individual roughness element would have to be considered.

For the sake of completeness, one should mention that in principle a similar no-slip condition at the wall could be imposed in case of a hydraulically smooth wall. This choice, however, would require a very fine grid to resolve the large gradients in the viscous sublayer near the wall (and a low-Reynolds formulation of the $k-\varepsilon$ model, see also APPENDIX A).

In order to economize grid points and thus save computer time and memory (and in order to prevent the use of a low-Reynolds formulation if the $k-\varepsilon$ model would be applied, see APPENDIX A), a different approach is often adopted. In the so-called wall function approach, the flow is resolved down to a first grid point (at $z = z_1$) away from the wall and well above the viscous sublayer. To bridge the gap between that point and the wall, use is made of some empirical wall function, like e.g.

$$\frac{U(z)}{u_*} = \frac{1}{\kappa} \ln\left(\frac{E u_* z}{\nu}\right).$$

(Note that many, more generalized relations have been proposed in literature.)

The wall function allows to determine the wall friction velocity u_*, and consequently the wall shear stress $\tau_w = \rho u_*^2$, as a function of the velocity U_1 (and in some generalized wall functions also as a function of the turbulent kinetic energy k_1) in grid point $z = z_1$.

If additionally is assumed that the first grid point away from the wall lies in the near-wall area where the shear stress is approximately constant (i.e. $30 \le u_* z_1/\nu \le 100$), then the Reynolds stress at $z = z_1$ (the gradient of which appears in the momentum equation for U_1) can be taken equal to the wall shear stress τ_w (which was expressed before as a function of U_1). Thus, the wall function approach allows to close the momentum equation at $z = z_1$ (and also define proper boundary conditions for k and ε at $z = z_1$, see APPENDIX F).

For more details, pro's and contra's of the approaches mentioned above, the reader is referred to the literature on turbulence modelling and its numerical simulation. See e.g. (Ferziger and Peric, 1996) and (Gatski, 1996).

APPENDIX F. TURBULENCE BOUNDARY CONDITIONS AT THE BED

Under the following assumptions:

- in the area close to the wall, the Reynolds stresses, $-\rho\overline{u'w'}$, are nearly constant and equal to the wall shear stress τ_w;
- thus (advection and) diffusion of turbulence is negligible and turbulence is said to be in local equilibrium ; consequently, the transport equation for k reduces to $\varepsilon = P$, which means that dissipation and production of turbulence kinetic energy balance out;
- in such an equilibrium turbulent boundary layer, the logarithmic velocity profile holds: $\frac{U(z)}{u_*} = \frac{1}{\kappa}\ln\left(\frac{z}{z_o}\right)$,

and based on the following definitions:

- the production of turbulent kinetic energy: $P = -\overline{u'w'}\frac{\partial U}{\partial z}$,
- the wall friction velocity: $u_* = \sqrt{\tau_w/\rho}$,
- the eddy viscosity: $\nu_t = c_\mu \frac{k^2}{\varepsilon}$,

one can derive the following boundary conditions for k and ε in case of a hydraulically rough flow:

$$k(z_o,t) = \frac{{u_*}^2}{\sqrt{c_\mu}},$$

$$\varepsilon(z_o,t) = \frac{{u_*}^3}{\kappa z_o}.$$

For the sake of completeness, one should mention that similar boundary conditions can be derived for hydraulically smooth flow if the wall function approach (see APPENDIX E) is applied in a first grid point (at $z = z_1$) away from the wall:

$$k(z_1,t) = \frac{{u_*}^2}{\sqrt{c_\mu}},$$

$$\varepsilon(z_1,t) = \frac{{u_*}^3}{\kappa z_1},$$

in which the wall friction velocity u_* can be expressed as a function of the velocity U_1 at $z = z_1$ by means of a 'wall function' like e.g. $\frac{U_1}{u_*} = \frac{1}{\kappa}\ln\left(\frac{Eu_*z_1}{\nu}\right)$.

APPENDIX G. GRID GENERATION

Be *N* the number of grid segments between levels z_o and z_∞. Let *R* denote the stretching factor, i.e. the height ratio of consecutive grid segments.

For $i = 0,$ define $z_O = z_o$ and for $i = N$ define $z_N = z_\infty$.

The first grid point away from the wall is then given by:

$$z_1 = z_o + (z_\infty - z_o)\frac{(1-R)}{\left(1-R^{N-1}\right)} \text{ (if R>1)}$$

$$z_1 = z_o + \frac{(z_\infty - z_o)}{N} \text{ (if R=1).}$$

The other grid points can be subsequently defined as follows:

$$z_i = z_{i-1} + R(z_{i-1} - z_{i-2}), \text{ for i=2,N.}$$

APPENDIX H. INITIAL CONDITIONS

In the present work, one can either start from an existing solution (i.e. the solution at the end of a previous boundary layer simulation, which has been written to a restart file) or one can adopt the following relations:

- a logarithmic velocity distribution in a turbulent flow: $U_i = U_{init} \dfrac{\ln\left(\dfrac{z_i}{z_o}\right)}{\ln\left(\dfrac{z_\infty}{z_o}\right)}$,
- a mixing-length formulation: $\nu_{ti} = \kappa z_i u_* = \kappa z_i \dfrac{\kappa U_{init}}{\ln\left(\dfrac{z_\infty}{z_o}\right)}$,
- a typical magnitude for the normal Reynolds stresses: $k_i = \dfrac{1}{2}\left(\overline{u'^2} + \overline{v'^2} + \overline{w'^2}\right) \approx \dfrac{1}{2}\left[3\left(\dfrac{U_{init}}{20}\right)^2\right]$,
- the eddy-viscosity definition: $\varepsilon_i = \dfrac{c_\mu k_i^{\,2}}{\nu_{ti}}$,

in which U_{init} is a user-specified current speed.

APPENDIX I. CONVERGENCE MONITORING

Be T_{cycle} the timescale at which the (oscillating) freestream flow, $U_\infty(t)$, can be considered to be periodic. The numerical timestepping procedure will then be carried out during a timespan equal to a multiple N_{cycle} of T_{cycle}.

For each cycle, T_{cycle}, the following quantities are calculated and presented to the user for the sake of convergence monitoring:

- the mean friction velocity over a cycle: $\frac{1}{T_{cycle}} \int_0^{T_{cycle}} u_*(t)dt$, in which u_* is taken equal to the product of the absolute value of the friction velocity and the sign of the velocity U_1 in the first grid point away from the wall,
- the maximum friction velocity (again taking into account the sign of U_1) over a cycle,
- the mean over a cycle of the instantaneous depth-averaged velocities: $\frac{1}{T_{cycle}} \int_0^{T_{cycle}} \left(\frac{1}{(z_\infty - z_o)} \int_{z_o}^{z_\infty} U(z)dz \right) dt$.

Other convergence indicators are feasible, however, and further experience with the present code might lead to another choice.

Note that at present, no stop-criterion is built-in in the code, i.e. the user-specified number of cycles (N_{cycle}) is carried out any way. Again, further experience with the code might lead to specification of stop-criteria if certain levels of convergence are reached.

REFERENCE LIST

1. Abbott,M.B., and Basco,D.R., 1989. Computational fluid dynamics – An introduction for engineers. Longman.

2. Al-Salem,A.A., 1993. Sediment transport in oscillatory boundary layers under sheet flow conditions. Ph.D. Thesis, Delft University of Technology.

3. Christofferson,J.B. and Jonsson,I.G., 1985. Bed friction and dissipation in a combined current and wave motion. Ocean Engineering, 12(5): 387-423.

4. Davies,A.G., Soulsby,R.L., and King,H.L., 1988. A numerical model of the combined wave and current bottom boundary layer. Journal of Geophysical Research, 93(C1): 491-508.

5. Dohmen-Janssen,C.M. Grain size influence on sediment transport in oscillatory sheet flow - phase lags and mobile-bed effects. Report No. 99-4. 1999. Delft, The Netherlands, Delft University of Technology - Faculty of Civil Engineering and Geosciences. Communications on Hydraulic and Geotechnical Engineering.
Ref Type: Report

6. Ferziger,J.H. and Peric,M., 1996. Computational methods for fluid dynamics. Springer.

7. Fredsøe,J., 1993. Modelling of non-cohesive sediment transport processes in the marine environment. Coastal Engineering, 21: 71-103.

8. Gatski,T.B., 1996. Turbulent flows: model equations and solution methodology. In: R.Peyret (Editor), Handbook of computational fluid mechanics. Academic Press, pp. 339-415.

9. Hirsch,C., 1988. Numerical computation of internal and external flows, Vol. 1. Wiley, New York.

10. Jensen,B.L., Sumer,B.M., and Fredsøe,J., 1989. Turbulent oscillatory boundary layers at high Reynolds numbers. Journal of Fluid Mechanics, 206: 265-297.

11. Justesen,P., 1988. Prediction of turbulent oscillatory flow over rough beds. Coastal Engineering, 12: 257-284.

12. Justesen,P., 1991. A note on turbulence calculations in the wave boundary layer. Journal of Hydraulic Research, 29(5): 699-711.

13. Li,Z. and Davies,A.G., 1996. Towards predicting sediment transport in combined wave-current flow. Journal of Waterways, Port, Coastal and Ocean Engineering, ASCE, 122(4): 157-164.

14. Rodi,W. Turbulence models and their application in hydraulics. State of the art paper. International Association for Hydraulic Research, Delft. 1984.
Ref Type: Report

15. Savioli,J.C. and Justesen,P., 1997. Sediment in oscillatory flows over a plane bed. Journal of Hydraulic Research, 35(2): 177-190.

16. Toorman,E.A. FENST-2D: a short description. Internal Report. 1997. Hydraulics Laboratory, Civil Engineering Dep., Katholieke Universiteit Leuven, Belgium.
Ref Type: Report

17. Toorman,E.A. Drag reduction in sediment-laden turbulent flow. Report No. HYD/ET/00/COSINUS5, MAST III COSINUS project. 2000c.
Ref Type: Report

18. Toorman,E.A. Parameterization of turbulence damping in sediment-laden flow. Report No. HYD/ET/00/COSINUS3, MAST III COSINUS project. 2000a.
Ref Type: Report

19. Toorman,E.A. Sediment-laden turbulent flow: a review of theories and models. Report No. HYD/ET/00/COSINUS1, MAST III COSINUS project. 2000b.
Ref Type: Report